Icarus 415 (2024) 116034

Contents lists available at ScienceDirect

Icarus

journal homepage: www.elsevier.com/locate/icarus

Lifetime of cm-sized zodiacal dust from the physical and dynamical evolution of meteoroid streams

Peter Jenniskens [a,b,*], Stuart Pilorz [a], Peter S. Gural [c], Dave Samuels [a], Steve Rau [d], Timothy M.C. Abbott [e], Jim Albers [a], Scott Austin [f], Dan Avner [g], Jack W. Baggaley [h], Tim Beck [i], Solvay Blomquist [g], Mustafa Boyukata [j], Martin Breukers [d], Walt Cooney [k], Tim Cooper [l], Marcelo De Cicco [m], Hadrien Devillepoix [n], Eric Egland [a], Elize Fahl [o], Megan Gialluca [g], Bryant Grigsby [a], Toni Hanke [o], Barbara Harris [p], Steve Heathcote [e], Samantha Hemmelgarn [g], Andy Howell [p], Emmanuel Jehin [q], Carl Johannink [d], Luke Juneau [r], Erika Kisvarsanyi [s], Philip Mey [t], Nick Moskovitz [g], Mohammad Odeh [u], Brian Rachford [v], David Rollinson [w], James M. Scott [x], Martin C. Towner [m], Ozan Unsalan [y], Rynault van Wyk [n], Jeff Wood [w], James D. Wray [a], Jérémie Vaubaillon [z], Dante S. Lauretta [aa]

[a] SETI Institute, 339 Bernardo Ave, Mountain View, CA 94043, USA
[b] NASA Ames Research Center, Mail-Stop 244-11, Moffett Field, CA 94035, USA
[c] Gural Software and Analysis LLC, 12241 Eliza Court, Lovettsville, VA 20180, USA
[d] CAMS BeNeLux, Am Ollenkamp 4, D 48599 Gronau, Germany
[e] CAMS Chile, Cerro Tololo Inter-American Observatory, NSF's National Optical-Infrared Astronomy Research Laboratory, Casilla 603, La Serena, Chile
[f] Dep. of Physics and Astronomy, University of Central Arkansas, 201 Donaghey Ave, Conway, AR 72035, USA
[g] LOCAMS, Lowell Observatory, 1400 West Mars Hill Road, Flagstaff, AZ 86001, USA
[h] CAMS New Zealand, Dept. of Physics & Astronomy, University of Canterbury, Christchurch 8140, New Zealand
[i] Mendocino College, 1000 Hensley Creek Road, Ukiah, CA 95482, USA
[j] CAMS Turkey, Yozgat Bozok University, Department of Physics, 66100 Yozgat, Turkey
[k] CAMS Texas, 4635 Shadow Grass Dr., Katy, TX 77493, USA
[l] CAMS South Africa, 258 Ninth Road, Bredell 1623, Kempton Park, South Africa
[m] CAMS EXOSS, Observatorio Nacional, Rua Gal. José Cristino 77, Rio de Janeiro, RJ 20921-400, Brazil
[n] CAMS Australia, Space Science and Technology Centre, Curtin University, Perth, WA 6102, Australia
[o] CAMS Namibia, High Energy Stereoscopic System Experiment, Windhoek 11009, Namibia
[p] CAMS Florida, Gainesville, FL 32605, USA
[q] CAMS Chile, STAR Institute, University of Liège, B-4000 Liège 1, Belgium
[r] CAMS Arkansas, North Little Rock, AR 72118, USA
[s] College of Central Florida, 3001 SW College Road, Ocala, FL 34474-4415, USA
[t] South African Radio Astronomy Observatory, HartRAO, Farm 502 JQ, Broederstroom Road, Hartebeesthoek 1740, South Africa
[u] UACN, International Astronomical Center, P.O. Box 224, Abu Dhabi, United Arab Emirates
[v] Embry-Riddle Aeronautical University, 3700 Willow Creek Road, Prescott, AZ 86301, USA
[w] Bindoon, WA 6502, Australia
[x] Department of Geology, University of Otago, P. O. Box 56, Dunedin 9054, New Zealand
[y] CAMS Turkey, Ege University, Faculty of Science, Department of Physics, 35100 Bornova, Izmir, Turkey
[z] IMCCE, Observatoire de Paris - PSL, 77 av. Denfert-Rochereau, 75014 Paris, France
[aa] Lunar and Planetary Laboratory, University of Arizona, Tucson, AZ 85721, USA

ARTICLE INFO

Keywords:
Meteors
Meteoroids
Comets, dust
Interplanetary dust

ABSTRACT

While comets eject mass mostly at cm-sizes and larger, that size range of particles is mostly absent from the interplanetary medium. Such particles are thought to be lost from the solar system by grain-grain collisions. Here, we investigate the lifetime of cm-sized meteoroids from their abundance in meteoroid streams of different age. For 487 streams, we measured the orbital element dispersions, the magnitude size distribution index, the

* Corresponding author at: SETI Institute, 339 Bernardo Ave, Mountain View, CA 94043, USA.
E-mail address: petrus.m.jenniskens@nasa.gov (P. Jenniskens).

https://doi.org/10.1016/j.icarus.2024.116034
Received 29 December 2023; Received in revised form 4 March 2024; Accepted 5 March 2024
Available online 9 March 2024

Interplanetary medium
Zodiacal light

ratio of fluffy and dense materials in the stream and their bulk densities, and the meteor light curve shape-parameter. We find that older long-period comet meteoroid streams tend to be more dispersed and evolve towards smaller semi-major axis, higher magnitude size distribution index, and contain relatively more high-density material. Meteoroids that approach the Sun closer than 0.2–0.3 AU are mostly young and composed of denser materials poor in sodium. We compare the observed properties of the streams to age estimates from the literature and to a set of new age estimates for long-period comet streams based on observed dispersions. We find that streams broaden with age inversely proportional to the perihelion distance (q). By selecting narrow ranges of age, we find that their magnitude distribution index changes proportional to $1/\sqrt{q}$, less steep than expected from meteoroid destruction by collisions. Instead, this shallow dependence suggests a lifetime inversely proportional to the peak grain temperature along its orbit, with the lifetime limited by thermal stresses if $0.3 < q < 1.02$ AU and by sublimation if $q < 0.2$ AU.

1. Introduction

Comets and primitive asteroids lose most mass in the form of grains that are centimeter (cm) to tens of cm-sized (e.g., Curdt and Keller, 1990; Levasseur-Regourd et al., 2018; Lauretta et al., 2019; Chesley et al., 2020). In contrast, the interplanetary (zodiacal) dust cloud that results from this mass loss (e.g., Nesvorny et al., 2010; Lasue et al., 2020) contains three orders of magnitude less mass at 1-cm than at 0.01-cm size (Love and Brownlee, 1993; Ceplecha et al., 1998). The total mass per log-mass interval of matter impacting Earth annually peaks at 0.015 cm and falls off by 2–3 orders of magnitude towards cm-sized meteoroids on the large size end, and even more towards the small size end where solar radiation pressure removes dust from the solar system (Fig. 1).

The lack of cm-sized meteoroids in the zodiacal cloud is usually explained by loss due to grain-grain collisions. With a constant supply of larger grains, the rate of collisions at different grain size ranges is at the heart of interplanetary dust models that describe the impact hazard to satellites in orbit (e.g., Grün et al., 1985; Divine, 1993; Soja et al., 2019; Moorhead et al., 2023) and the overall appearance of the zodiacal cloud (e.g., Nesvorny et al., 2010).

In the Grün et al. (1985) grain-grain collision model, the mass dependence of the influx rate of meteoroids on a spinning surface at Earth's orbit is analytically described by assuming a collisional equilibrium among interplanetary meteoroids and a specific mechanism of grain destruction. Target particles with mass m_1 are assumed to be catastrophically disrupted, whereby the largest fragment is half the size of the original mass, by particles of given impact speed V (km/s) that exceed a minimum mass m_2 (and corresponding kinetic energy):

$$m_2 \geq 0.00102\ S_c^{0.45}\ \rho_1^{0.075}\ V^{-2}\ m_1^{0.925} \quad (1)$$

with S_c the unconfined compressive strength (kbar) and ρ_1 the target meteoroid density (g/cm^3).

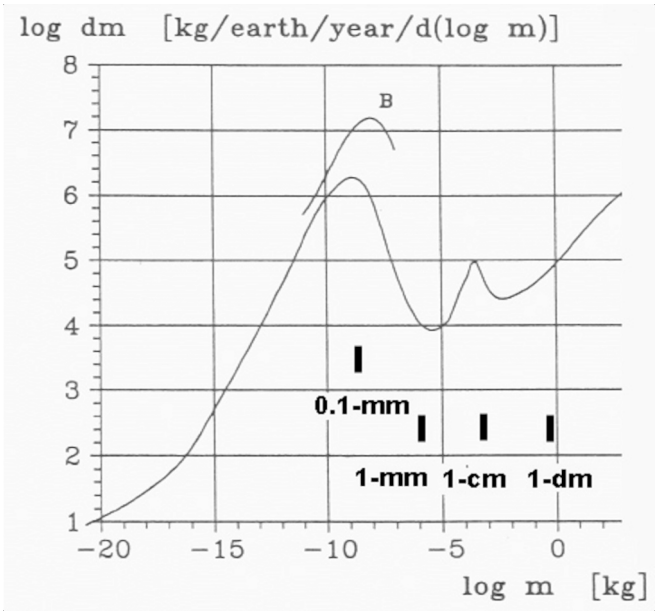

Fig. 1. Mass influx curve from Ceplecha et al. (1998), with approximate size markers added. Curve "B" is the influx profile proposed by Love and Brownlee (1993).

This collision model makes distinct predictions about how the meteoroid lifetime depends on mass (Table 1). In this model, the 0.015-cm grains at the peak of the max influx curve are preferably destroyed by the comparatively few small grains of mass 10^{-13} kg (which in Fig. 1 have low total mass and therefore low total kinetic energy), while the larger 1-cm grains are destroyed by the abundant 10^{-8} kg meteoroids. The collisional lifetime increases again for larger grains, because the number density of the projectile meteoroids is less. In this model also, higher inclined orbits tend to have about a factor of two longer collisional lifetimes because they spend less time at the core of the interplanetary dust cloud near the ecliptic plane.

Using the same collisional model as Grün et al. (1985), but applied to a modern meteoroid environment model of dust densities and impact velocities, Soja et al. (2016) calculated a collisional lifetime of 30,000 years for 0.01-cm grains and 2500 yr for 1-cm grains that are moving on a short-period comet 2P/Encke-like orbit, and about 10 times higher lifetimes for dust on a 55P/Tempel-Tuttle orbit (Table 1). Lifetimes are assumed to increase exponentially for the smallest grains with mass less than $\sim 10^{-16}$ kg. The mass-dependence of this relationship is independent of the meteoroid orbit.

Important, too, are the dynamical lifetimes of the grains. Submicrons sized grains are put on unbound orbits by solar radiation pressure. The drop-off towards small sizes in Fig. 1 was thought to be due to Poynting-Robertson drag, decreasing eccentricity over time and causing meteoroids to spiral in towards the Sun. However, small mm-sized grains on near-circular orbits in the asteroid belt require longer than the age of the zodiacal cloud to reach Earth's orbit (e.g., Nesvorny et al., 2010; Haranas et al., 2018).

The lifetime of the grains may not be limited by collisions or dynamics. Fig. 2, for example, shows the rate of Leonid storms and outbursts from 1333 CE to 1932 ejecta from Halley-type comet 55P/Tempel-Tuttle, predicted from two models by E. Lyytinen and J. Vaubaillon published in Jenniskens (2006) and Jenniskens et al. (2008, 2009), and compares those predicted rates to the observed values. The predicted activity is scaled to the encounters with the young 1–4 revolution dust trails. The predictions assume a constant activity of the comet in each return and include all possible dynamical effects. The models systematically predict higher rates than observed in the case of older trails, with the ratio showing an e-folding scale of 259 ± 17 y (Fig. 2, dashed line). That rate is a factor of 4–10 more rapid than expected from grain-grain collisions (Table 1). While the comet could also have become correspondingly more active over time, this is less likely because the perihelion distance has not significantly decreased since 1333 CE (Yeomans et al., 1996) and the ratio does not correlate with the comet's perihelion distance during ejection.

Processes other than collisions can act on different timescales for different grain morphologies and strengths. Indeed, some Leonid meteoroids survive and evolve into an annual Leonid shower over a much longer timescale (Jenniskens, 2006). Further evidence for meteoroid fragmentation in the interplanetary medium by processes other than collisions are the relatively frequently observed clusters of meteors observed from the breakup of 1–10 cm sized meteoroids just before reaching Earth, which have been ascribed to thermal stresses (e.g., Piers and Hawkes, 1993; Koten et al., 2017, 2024; Vaubaillon et al., 2023).

On very short timescales, dust bursts observed by the Rosetta mission to comet 67P/Churyumov-Gerasimenko show that some mm- and cm-sized grains fragment into smaller grains while ice is sublimating from the grains (e.g., Fulle et al., 2018). Clusters of dust were also observed in the flyby's of the 81P/Wild 2 and 9P/Tempel 1 comae (Levasseur-Regourd et al., 2018). It is the ice-free grains that survive which form the cometary dust trails and subsequently evolve into annual streams and the zodiacal cloud.

Cometary meteoroids are porous and diverse and, importantly, a mixture of aggregates and compact particles (Langevin et al., 2016; Bentley et al., 2016). Derived dust densities were between 0.05 and 0.5 g/cm^3 in the coma of comet 1P/Halley (Fulle et al., 2000), and <1 g/cm^3 for other encounters (Levasseur-Regourd et al., 2018). Short-period comet 67P particles had a bulk density of 0.7–1.4 g/cm^3 (Fulle et al., 2017), centered on 0.8 g/cm^3. Some particles are extremely fluffy (>90% porosity), while compacted and dried particles had density 1.3–3.9 g/cm^3, centered on 1.9 g/cm^3. Collected particles of 81P/Wild 2 contained small particles of different tensile strength (Brownlee et al., 2006). Cometary dust contains organic components (~45% in mass for comet 67P, Bardyn et al., 2017) and amorphous silicates, but also crystalline silicate materials that experienced some heat in the past (Crovisier, 1997; Wooden et al., 1999). About half of the silicates in 81P/Wild 2 samples were crystalline, and ~ 1% are highly refractory minerals reminiscent of Calcium-Aluminum-rich Inclusions (Westphal et al., 2009).

The grains that survive long enough to become part of a zodiacal dust cloud do not fully behave as predicted by the Grün et al. model. To explain the observed infrared emission, dynamical models of the interplanetary dust cloud require about the same collisional lifetimes for 0.1-cm particles as for 0.01-cm particles (Nesvorny et al., 2010, 2011; Pokorny et al., 2014). The ~0.1-cm sized meteoroids in the sporadic background observed by the Canadian Meteor Orbit Radar CMOR (Brown et al., 2010) move on similar orbits as the ~0.01-cm sized grains observed by the more sensitive AMOR radar (Galligan and Baggaley, 2002). Both populations seem to be about 300,000 years old (Nesvorny et al., 2010), but the Grün et al. model predicts about 7 times higher lifetimes against collisions for the smaller 0.01-cm AMOR radar particles than the 0.1-cm CMOR particles (Table 1).

The smaller particles also should evolve faster by Poynting-Roberston drag. To match the AMOR orbits, the CMOR meteoroids require 3 times more drag than expected for the collisional lifetime available. Even smaller ~10 μm grains that scatter light to create the visible zodiacal light do not impact Earth on near-circular orbits from Poynting-Robertson drag as predicted in earlier zodiacal cloud models, but on orbits of eccentricity e ~ 0.3, based on relatively wide Doppler broadened spectral features in the zodiacal cloud (e.g., Reynolds et al., 2004; Rowan-Robbinson and May, 2013) and the relatively high impact speeds inferred from helium loss in interplanetary dust particles (e.g., Flynn, 2001). While Poynting-Robertson drag lowers the eccentricity over time, some mechanism appears to remove the grains before their orbits can fully circularize.

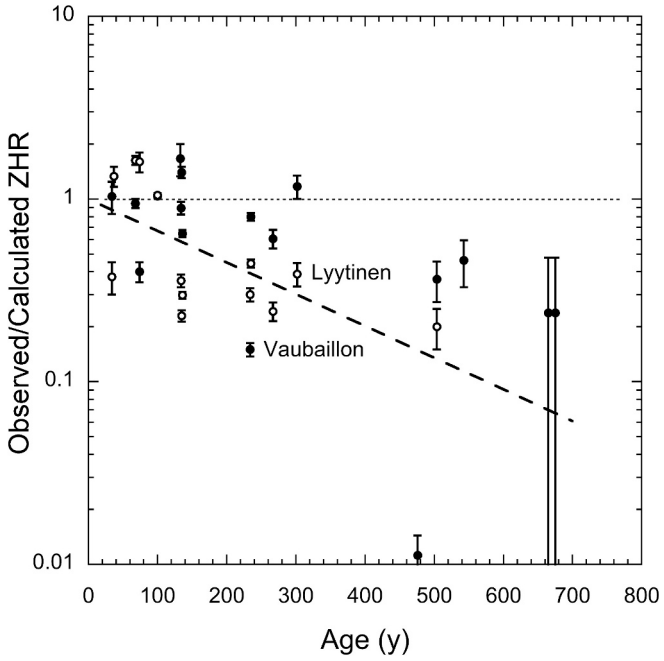

Fig. 2. Ratio of observed versus predicted Leonids meteor shower activity, with predicted activity from the models by Vaubaillon (•) and Lyytinen (o) published in Jenniskens (2006) and Jenniskens et al. (2007; 2009).

There are other ways than grain-grain collisions to remove large grains from the population. For example, repeated cycles of heating and cooling could disrupt a meteoroid over time by loosening bonds or creating tension. The spin rate of a meteoroid could increase to the point where centrifugal forces disrupt the grain, and repulsive electrical forces could build up over time when the grains are charged by radiative processes. Such mechanisms will display a different mass-dependence of lifetimes and a different dependence on radial distance from the Sun and vertical distance from the ecliptic plane.

To test the importance of these mechanisms in removing cm-sized grains from meteoroid streams and the zodiacal cloud, it is necessary to do meteor observations. These cm-sized meteoroids do not efficiently emit infrared radiation or scatter sunlight for direct observations, and also cannot be detected by the small dust collectors onboard spacecraft.

From low-light level video observations of meteor showers caused by cm-sized meteoroids (Jenniskens et al., 2011), we derived the dispersions of 487 meteoroid streams, as well as the particle size distribution, the altitude at which 0-magnitude meteors first light up in the atmosphere, and the meteoroid density from deceleration in the atmosphere. The raw data was published in the book "*Atlas of Earth's Meteor Showers*" (Jenniskens, 2023).

Here, we use this data to investigate how the particle size

Table 1
Calculated and observed lifetimes of meteoroids in the zodiacal cloud.

Diameter (cm)	Mass* (g)	Magn. (V)	Lifetime calc. (ky)	Ref.	Lifetime obs. (ky)	Method	Ref.
0.001	1e-9	+22.5	1600	[1]	-.-	-.-	-.-
0.01	1e-6	+15	269	[1]	~300	IR, zodiacal cloud dynamical model	[2]
0.1	1e-3	+7.5	40	[1]	≥300	IR, zodiacal cloud dynamical model	[2]
1	1e+0	+0	13	[1]	-.-	-.-	-.-
10	1e+3	−7.5	440	[1]	-.-	-.-	-.-

Notes: [1] For Grün model of 2 g/cm^3 particles on a 55P/Tempel-Tuttle (q ~ 1 AU) orbit; Soja et al. (2016, 2019); *) for density of 2 g/cm^3; [2] Nesvorny et al. (2010).

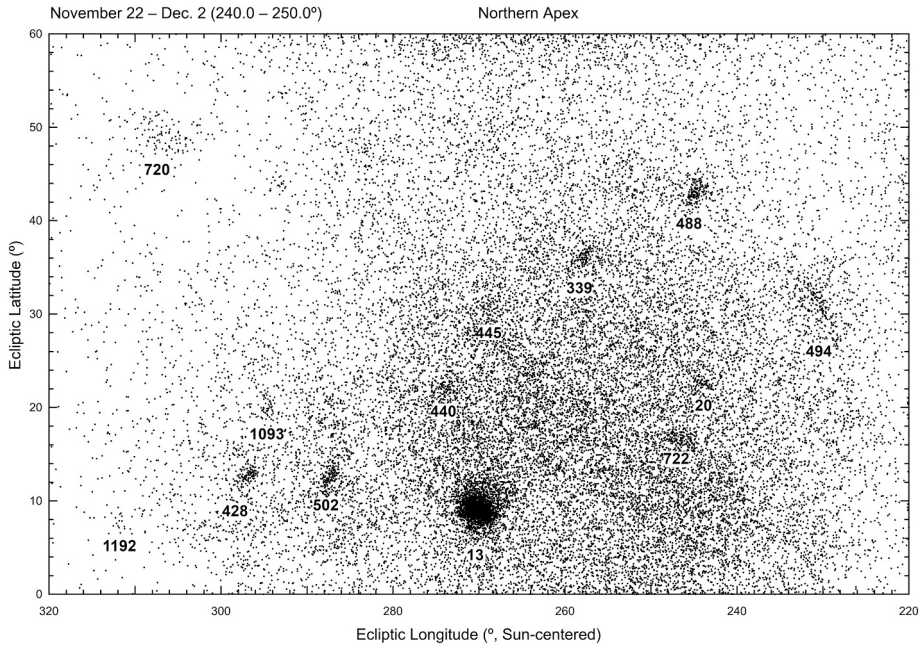

Fig. 3. Example of meteor showers (labeled with their IAU number) in the radiant distribution towards the northern apex direction during solar longitudes 240° to 250° (Nov. 22 to Dec. 2). From: Jenniskens (2023).

distribution, the meteor light curve, the meteoroid density, and the ratio of fluffy to dense materials change with age, both as a function of perihelion distance and inclination of the meteoroid orbit. Some age estimates were taken from the literature. For a range of long period comet orbits, we investigated the stream dispersion over time. From the observed changes over time, we will discuss what mechanisms may be responsible where for the loss of cm-sized grains in the interplanetary medium.

2. Methods

2.1. Meteoroid streams observed as meteor showers

The Cameras for Allsky Meteor Surveillance (CAMS) project (Jenniskens et al., 2011) deploys networks of low-light video cameras in different regions of the world to detect and triangulate the atmospheric path of +4 to −5 magnitude meteors and calculate meteoroid trajectories, initial velocity and orbits, as well as light curves, decelerations, and meteor magnitude distributions. The network was significantly expanded in the southern hemisphere in 2019.

From 2010 to 2023, CAMS triangulated over 2.7 million meteoroid trajectories. From clusters in the distribution of meteor arrival time, radiant and speed (e.g., Fig. 3), individual showers were extracted and median orbital elements were published by Rudawska and Jenniskens (2014), Jenniskens et al. (2016a–c), Jenniskens and Nénon (2016), and Jenniskens et al. (2018). This database was again examined for clusters using the same methods as before (Jenniskens et al., 2016c, 2018), after adding the most recent data up to July 3, 2023, after adding about 1.1 million other published meteoroid trajectories derived by the SonotaCo (Kanamori, 2009), EDMOND (Kornos et al., 2013), CMN (Adreic and Segon, 2010), and GMN (Vida et al., 2020; 2021) networks. In all, 122 new showers were added to the IAU Working List as numbers 1050–1108, 1110, 1129–1130, 1132–1178, and 1180–1192. While working on Jenniskens (2023), the process for shower naming was changed, in which the assignment of numbers, codes and names was postponed until an undefined later time. In order to be able to include these in Jenniskens (2023), eight additional showers were given the provisional numbers 674, 676, 678, 682, 690, 697, 699 and 700, previously assigned but not used for Jenniskens et al. (2016a), as well as codes and names. In all, 23% of video-detected meteors belong to 487 identified meteor showers, while another 26 showers described in Jenniskens (2023) are only detected by radar.

The meteoroid orbit at the time of entry can be calculated by tracking the meteoroid's motion along its path through the atmosphere, expressed as orbital elements perihelion distance (q), eccentricity (e), inclination (ι), argument of perihelion (ω), and longitude of the ascending node (Ω) (Jenniskens et al., 2011). Hereinafter, the longitude of ascending or descending node will be referred to as node. For the extracted orbits of each meteoroid stream, the median values of these orbital elements are calculated, as well as the 1-σ dispersion (σ), and the rate of change in the orbital elements as a function of solar longitude along Earth's path (the orbital element drift). Jenniskens (2023) gives the dispersion in orbital elements rather than the radiant dispersion, which depends on entry speed (e.g., Tsuchiya et al., 2017).

The dynamic type of a meteoroid orbit follows from its Tisserand's parameter with respect to Jupiter:

$$T_J = a_J / a + 2\cos(i)\ \sqrt{a/a_J\,(1-e^2)} \qquad (2)$$

with a_J the semi-major axis of the orbit of Jupiter. Parent bodies are typically described as long-period comets having ($T_J \leq 1$), Halley-type comets ($1 < T_J \leq 2$), Jupiter family comets ($2 < T_J \leq 3$), and asteroids having ($T_J > 3$).

2.2. Average physical properties of the meteoroids in showers

These optical observations pertain to meteoroids of diameter about 0.7–cm for fast showers from the apex source, and to about 1.8-cm for slow showers from the anthelion source (Fig. 4). Once a shower has been extracted from the sporadic background, the properties of the individual meteors in that shower can be examined.

How those parameters were extracted is given in Jenniskens (2023). In short, the magnitude distribution index (χ) describes the ratio of how many meteors are in neighboring magnitude bins of brightness. The observed count (N) per magnitude bin (m) depends on the detection probability for each magnitude P(m):

$$N(m) = P(m)\,\chi^m \qquad (3)$$

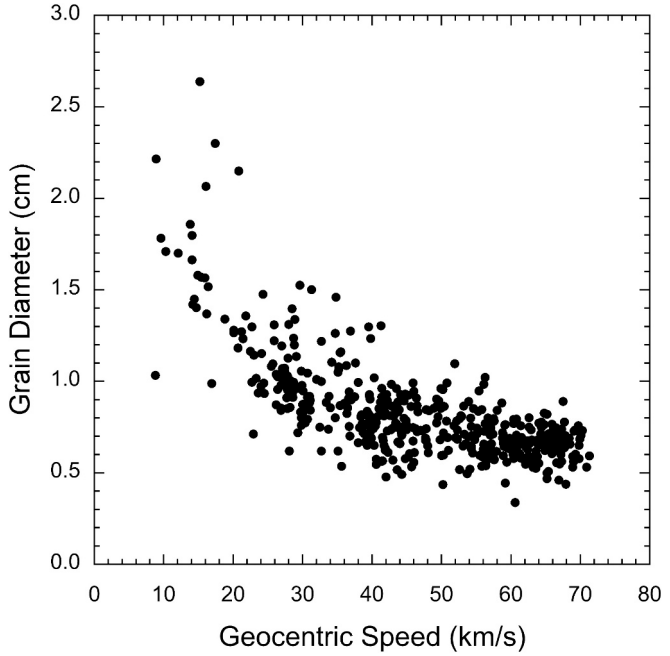

Fig. 4. Median grain diameter of a zero-magnitude meteor for all showers over the full range of entry speed. Vertical dispersion is due to differences in the measured meteoroid density.

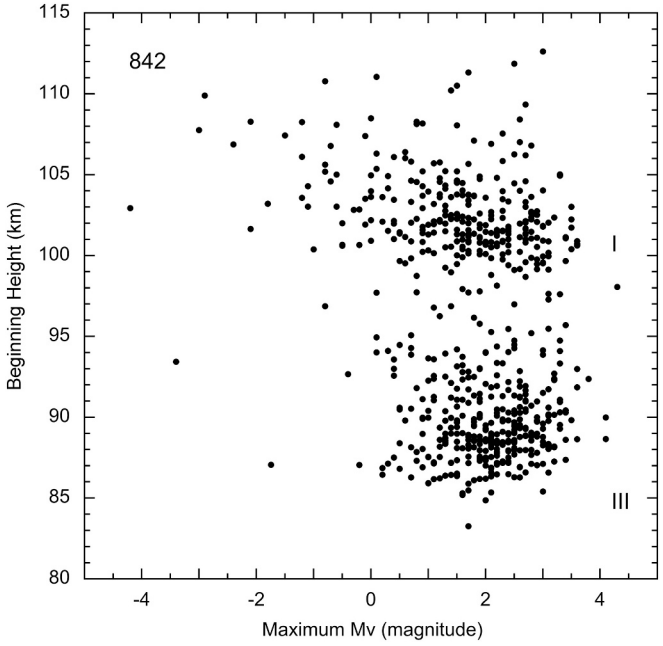

Fig. 5. Beginning height of all shower IAU#842 meteors triangulated by CAMS cameras. Symbols "I" and "III" indicate the two main meteor beginning-height classes present in the shower.

The mass distribution index $s = 1 + 2.5 \log(\chi)$. While nearly all meteors brighter than +0 magnitude are detected, few faint meteors are. This is mainly because the contributing stations in a triangulation are often at different distances from the meteor and meteors are fainter when further away. Also, fast meteors tend to move rapidly over the sensor and are less efficiently detected. Meteors slower than 20 km/s are also more easily missed. In addition, the detection efficiency of a given shower depends on whether it can be detected by southern hemisphere stations, which have newer cameras on average and are located under darker skies. When CAMS-detected rates were high enough to populate the bright −4 to −1 magnitude range, where $N(m) \sim \chi^m$, then χ could be derived directly. Extrapolation to fainter +5 magnitudes resulted in the observed versus expected number ratio P(m). In this way, probability functions were derived for a range of entry speed and shower radiant latitude. If a minor shower had a radiant near one of the calibrated showers, then that efficiency curve was used.

Each meteor has a beginning height where it is first detected (H_{begin}), a height of peak brightness (H_{max}), and an end height (H_{end}). The lightcurve shape parameter is defined as (e.g., Beech and Murray (2003)):

$$F = (H_{max}–H_{begin})/(H_{end}–H_{begin}) \quad (4)$$

The shape factor is a low $F \leq 0.59$ if the meteoroid is fragile, while $F \sim 0.76$ if the meteoroid is a single body.

Looking at the beginning heights of meteors in a given shower, there is a range of values (Fig. 5). Often, there are two groups in a shower, a group that is first detected at a relatively high altitude (I) and a group that is only detected further down (III). The orbital elements of each group are the same, hence particles with these different beginning heights belong to the same stream. Differences in beginning height are expected for meteoroids of different density, different thermal conductivity, but also different strength (Ceplecha and McCrosky, 1976). Our spectroscopic measurements of meteors show that the lower group is associated with meteors poor in sodium (Jenniskens, 2023), meaning that these grains experienced sufficient heating to lose some of the sodium-containing minerals. Heating tends to result in an increase in strength and an increase in density. Hence, throughout this paper we will refer to these groups as "fluffy" or "low density" (I) and "dense" or "high density" (III). While the number of members in each group depends on the activity of the shower, the ratio of members in the two groups, e.g. III/(I + III), is diagnostic for the process that created the type III particles.

The beginning height is to first order dependent on the square of the entry velocity (V_∞). After correcting for this effect, we define a *beginning height parameter* k_c as:

$$H_b\ (km) = k_c\ (km) – [2.86–2.00\ log\ (V_\infty\ (km/s))]/0.0612 \quad (5)$$

The equation is written this way because the air mass density ρ_{air} as a function of height over the full 0 to 150 km range is approximated by (Ceplecha and McCrosky, 1976; Jenniskens, 2023):

$$^{10}log\ \rho_{air}\ (g/cm^3) = −2.86 − 0.0612\ H\ (km) \quad (6)$$

Values of k_c (valid for $M_v = 0$ meteors) are mostly in the narrow range of 85–103 km. The range of k_c was divided up in three-km bins, from which meteors were assigned to belong to type Ia, I, Ib, IIa, II, IIb and IIIa, IIIb, and IV (Fig. 6). They are shown with these symbols throughout the paper. The numbering (from high to low beginning altitudes) is opposite to that used in the classification by Ceplecha and McCrosky (1976), which may help avoid confusion.

Roughly, showers Ia–II are part of band I in Fig. 5, while IIb–IV are part of band III. We added the number of meteors in the subclassifications Ia to II into a "low-density" or "fluffy" class, and the number of meteors in the subclassification IIb to IV into a "high-density" or "dense" class (Fig. 6). The fraction of dense meteoroids in the population was determined from the number of meteors with low beginning height over the total III / (I + III):

$$f_d = N(IIb–IV)/N(Ia–IV) \quad (7)$$

Defined in this manner, f_d ranges from 0 to 1.

The meteoroid density was derived from the measured deceleration parameters a_1 (unit: km) and a_2 (unit: /s), defined as (Jacchia et al., 1967):

$$V = V_\infty + a_1\ a_2\ (1 − exp(a_2 t)) \quad (8)$$

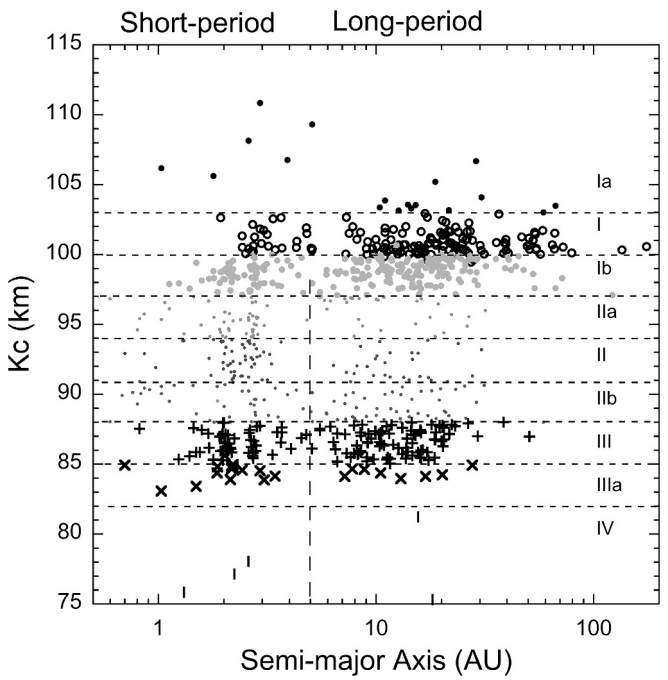

Fig. 6. The median beginning height of all CAMS-detected meteor showers, corrected for velocity-dependence (K_c). Different symbols (used in later graphs) define 3-km bins in the K_c-heights distribution and correspond to the shower type Ia – IV, as defined by Jenniskens (2023).

Here we should point out that not all CAMS data were reduced with this type of fit. The software allows for three options for the deceleration fit and sometimes another option was set by mistake, usually following the manual analysis of a fireball that required a different fit. The reported deceleration parameters were sorted to only include the ones reduced with Eq. 8.

We assume that the luminous efficiency does not depend on speed. If it does (e.g., Koschny et al., 2017), then the dependency of beginning height with entry speed would be different than observed. In that case, the mass (m) of a zero magnitude ($M_v = 0$) meteor is derived from the emitted energy being equal to the energy passing through a sphere at a distance from:

$$\tau \times 0.5 \times m \times V_\infty^2 = 3.67.10^{-11} \times \Delta t \times \Delta\lambda \times 4\,\pi\,R^2 \quad (9)$$

with $3.67.10^{-11}$ W/m^2/nm being the V-band irradiance of magnitude 0 star Vega (Jenniskens, 2006), Δt the meteor duration, $\Delta\lambda$ the full-width-half-maximum range in wavelength covered by the camera, R the distance from camera to meteor and V_∞ the entry speed. The duration Δt of a zero-magnitude meteor in CAMS data depends on V_∞ as $\Delta t \sim V_\infty^{-0.73}$ (by plotting the observed values of log Δt vs. log V_∞). This makes the mass of a zero-magnitude meteor proportional to $m \sim V_\infty^{-2.73}$.

The density of the meteoroid (ρ) follows from the transfer of momentum from air with density ρ_{air} to the meteoroid. During Δt, a meteoroid with speed V and mass m will strike a mass of air $m_{air} = A_E\,\rho_{air}\,V\,\Delta t$. The deceleration to first order (from Taylor expansion of Eq. 8) at the beginning of the trajectory is (with ρ_{air} the air density at the beginning altitude):

$$\delta V/\delta t = -0.5\ Cd\ A_E/m\ \rho_{air}\ V_\infty^2 = -a_1 \cdot a_2^2 \quad (10c)$$

For a spherical grain with radius r: $m = A_E\,\rho\,r\,/\,3$, so that.

$$\rho \sim \rho_{air}\ V_\infty^2/(a_1\ a_2^2\ r) \quad (10b)$$

If we use the beginning height of 0-magnitude meteors only, and taking into account that the mass of a zero-magnitude meteor scales with $V_\infty^{-2.73}$, in that case we have $r \sim V_\infty^{-2.73/3} = V_\infty^{-0.91}$ and the bulk meteoroid density (ρ) scales with (Jenniskens, 2023):

$$\rho \sim \rho_{air}\ V_\infty^{2.91}/(a_1\ a_2^2) \quad (10c)$$

The scale was chosen so that the highest densities measured were that of molten silicate droplets (3.5 g/cm^3). While there are higher density iron particles in the cm-sized meteoroid population, at a rate of 21 such Fe particles detected among 1005 random meteors (Jenniskens, 2023), they are not associated with meteor showers.

The results can be compared to the rigorously determined meteoroid densities from high temporal and high spatial resolution imaging and lightcurves of cometary meteoroids. The approach above puts the October Draconid density at 0.28 g/cm^3 (measured from lightcurves: 0.30 g/cm^3 by Borovicka et al., 2008), the tau-Herculids at 0.28 g/cm^3 (0.26 g/cm^3 by Buccongello et al., 2023, 2024, using the same method as Borovicka et al., 2008), the eta-Aquariids and Orionids at 0.41 g/cm^3 (~0.40 g/cm^3 by Buccongello et al., 2023; 0.26 ± 0.11 by Buccongello et al., 2024), the Lyrids at 0.41 ± 0.07 (0.44 ± 0.05 g/cm^3 by Buccongello et al., 2024), the eta-Lyrids at 0.78 g/cm^3 (0.86 g/cm^3 by Buccongello et al., 2024), the Southern Taurids at 1.38 ± 0.05 (0.68 ± 0.17 g/cm^3 by Buccongello et al., 2024), and the Geminids at 1.27 g/cm^3 (1.39 ± 0.24 g/cm^3 by Buccongello et al., 2024).

2.3. Meteoroid stream models

To investigate the changes over time in the parameters discussed in Sect. 2.2, we investigated the age of long-period comet showers in our sample, which comprise of almost half of all showers. To date, there are very few published dynamical studies of long-period comet showers and the studies that have been published are not focused on how the showers disperse as a function of time, but rather how the complex can evolve to created multiple showers (Hajduková et al., 2015; Hajduková and Neslusan, 2017, 2019, 2021; Neslusan and Hajduková, 2018, 2019, 2020, 2021).

The theoretical work follows methods developed by Vaubaillon et al. (2005), Jenniskens (2006) and Jenniskens and Vaubaillon (2010), taking into account the planetary perturbations of all the planets from Mercury to Pluto as well as radiation pressure, solar wind pressure and Poynting-Robertson drag on the meteoroids. Orbital elements of known comets were used during testing. Integrations were carried out on a Dell Precision 7820 Tower Workstation dedicated to this project. The techniques used have been successfully applied in the past (e.g., Vaubaillon et al., 2005; Wiegert et al., 2009; Moorhead et al., 2014; Abedin et al., 2015; Tomko and Neslusan, 2019).

The PINTEM code by Vaubaillon et al. (2005) was adapted to speed up the integrations and remove redundancies. This code is built around a 15th order implicit Bulirsch–Stoer-like routine (Everhart, 2014). Comparisons of integrated orbits with NAIF SPK kernels for known comets indicated that requiring convergence to 14 or 15 digits was attainable. With less than that, the exchange of kinetic and potential energy around perihelion is slightly different than that obtained using NAIF kernels. The code is configured now to run with either the SPICE library and NAIF SPK kernels (Acton et al., 2017), or with the Calceph library and INPOP files (Gastineau et al., 2015; Fienga et al., 2008). The latter are necessary for longer period integrations that extend beyond the 15,000 years that the JPL De441 kernels allow.

Comet 55P/Temple-Tuttle was used for validation of short term integrations, with good agreement obtained with previous studies by McNaught and Asher (1998) and Vaubaillon et al. (2005) using NAIF kernels. The z-plane crossing locations for ejecta streams from all perihelia from 1699 to 1965 were compared, and the width and temporal profile of streams were analyzed, in order to catalog the mass distribution versus time for streams of various ages.

For longer integrations, our workhorses are two 500kyr INPOP ephemerides centered on the present, and readable with the Calceph library (Gastineau et al., 2015). Our implementation of the Calceph

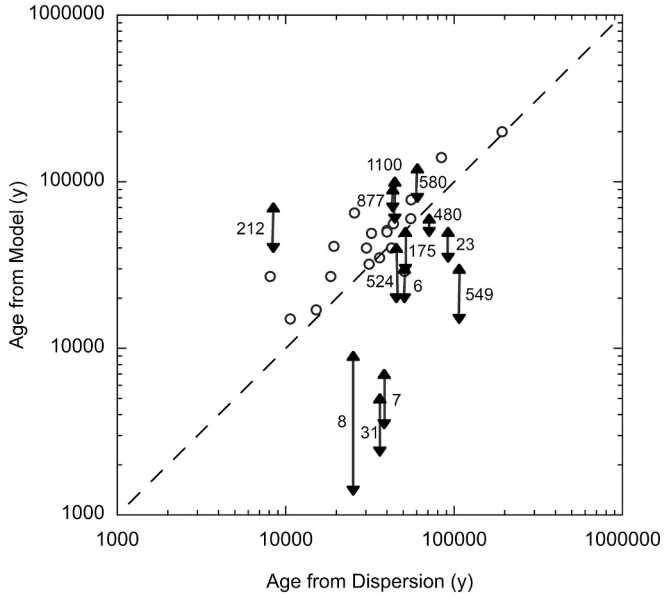

Fig. 7. Age estimates for long-period comet showers based on dynamical models of meteoroid stream dispersions (o, Table 5). Triangles show ages derived from published work (as listed in Jenniskens, 2023).

library was checked by finding consistent agreement between integrations performed from 10,000 BCE to the present for a number of initial conditions, using the Calceph library and ephemerides versus using the SPICE library with the NAIF de441 kernel.

The method to study the dynamical evolution of meteoroid streams (e.g., Kondrat'eva and Reznikov, 1985; Harris et al., 1995; Vaubaillon et al., 2005; Jenniskens, 2006) focuses on quantifying the growth in dispersion of the stream particles' orbital elements as the stream is integrated forward in time. Initial conditions are found by first integrating the orbit of the parent body, or of a body with the stream's orbital elements when the parent body is not known, back in time for 60,000 to 100,000 years. We adopt initial orbits with orbital periods between 250 and 4000 years, similar to that of known dynamically long-period comets with observed showers (Jenniskens et al., 2021). Comets on longer orbital periods have streams too dilute to be detected. Non-gravitational forces are taken into account only if they are tabulated in the NAIF Small Bodies database.

Fig. 7 shows our calculated ages for long-period comet showers by matching the observed stream dispersion in Earth's path to that modeled as a function of age (open circles, Table 5 below). The derived ages are plotted against ages calculated from a general equation based on dispersion (Jenniskens (2023). We tend to find similar, on average ~ 27% higher, ages than derived from other work (dashed line). Solid triangles show results from comparing observed dispersions to those calculated for different ages in graphs published by Hajduková et al. (2015), Hajduková and Neslusan (2017, 2019, 2021), and Neslusan and Hajduková (2018, 2019, 2020, 2021). Showers are identified with the IAU shower number. The age of the Orionids (8), eta-Aquariids (31) and Perseids (7) are discussed in the "Brief history" sections in Jenniskens (2023) and may be higher than given here.

3. Results: Shower properties and dependencies

3.1. Detected streams

A total of 487 meteor showers were extracted from the video data, while 26 additional showers were identified unique to radar. The nature of these showers is shown in Fig. 8A, which plots the median orbital inclination versus semi-major axis. Nearly half of the showers (247) originated from long-period and Halley-type comets. These showers have semi-major axis larger than 5 AU and inclinations between 20 and 180°. Short-period showers (semi-major axis < 5 AU) are mostly found in the anthelion and helion sources (inclination <20°) and in the toroidal sources (inclination 20–90°). The radar-detected showers are mostly short-period showers in the helion and toroidal sources, as well as some strong Halley-type showers (open circles in Fig. 8A). The showers unique to radar are not considered here.

Fig. 8B plots the orbital elements in terms of the Tisserand parameter with respect to Jupiter. The traditional distinctions between asteroids ($T_J > 3$), Jupiter family comets ($2 < T_J < 3$), Halley-type comets ($1 < T_J < 2$), and long-period comets ($T_J < 1$) are also recognized, but the borders are slightly different because the meteoroid streams have evolved over time. Solid lines in Fig. 8B show the approximate new borders.

The dynamic type of a meteoroid stream is long-period comet like for $T_J < 0.65$, Mellish-type for $0.65 < T_J \leq 2.0$, Jupiter-family comet type $2.0 \leq T_J \leq 3.5$, and asteroid like for $T_J > 3.5$. The borders reflect the observed distribution of median Tisserand parameters of meteor showers, not the dynamical class of the parent body.

"Mellish-type" showers are mostly prograde highly inclined (i = 20–80°) showers in the toroidal source. The December Monocerotids of comet C/1917 F1 (Mellish) is the lowest-numbered example. Dynamical models suggest they originated mostly from Halley-type comets, but can also originate from Jupiter-family comets, and even from asteroids. Halley-type comets 1P/Halley, 109P/Swift-Tuttle, and 55P/Tempel-Tuttle have "Long-period comet" type meteor showers (Jenniskens, 2023). The "toroidal source" consists of short-period meteoroids in highly inclined $\iota \sim 60°$ orbits, and is named this way because these orbits form a cylindrical toroid in space (Hawkins, 1963).

We notice here that many Jupiter-family comet showers come as a group that evolves smoothly from the Mellish-type group into the asteroidal group. Examples are the showers from the Machholz Complex for 96P/Machholz. Other Jupiter-family comet showers scatter to higher Tisserand parameters, with higher semi-major axis and having evolved less since capture by Jupiter.

The meteoroid streams of primitive asteroids have similar Tisserand parameters to the evolved Jupiter-family comets. Based on identified parent bodies, only a few showers appear to have originated from primitive asteroids, and most of those have low perihelion distance (Jenniskens, 2023).

Long-period comet streams are detected from parent comets with orbital periods in the range from 250 to 4000 y (Jenniskens et al., 2021). Those streams come in two different dynamical groups. Fig. 9 shows that most retrograde moving streams have a value of the rate at which the argument of perihelion (ω) changes along Earth's path follows a strong function of the inclination of the orbit (Jenniskens, 2023). This group defines a class of parent bodies that are perturbed by planetary perturbations in a systematic way, showing mostly the effect of precession and conditions needed for the meteoroids to intersect Earth's orbit. A similar but weaker effect is seen in the drift of the perihelion distance versus inclination.

3.2. Measured dispersions

Fig. 10A–C show the measured dispersions as a function of their values in the orbital elements node (Ω), argument of perihelion (ω), and inclination (ι). The dispersions describe the 1-sigma spread in the orbital elements, after correcting for daily drift along Earth's path. The dispersions in node were corrected for the geometry of the encounter, showing Ω * sin (δ), where the attack angle δ is given by:

$$\delta = 180^{\circ} - arccos(sin(\lambda - \lambda_o)\ cos(\beta)\ ) \quad (11)$$

with λ and β the ecliptic longitude and latitude of the radiant and λ_o the solar longitude. The dashed lines in Fig. 10A and B show prograde ($\iota \leq$

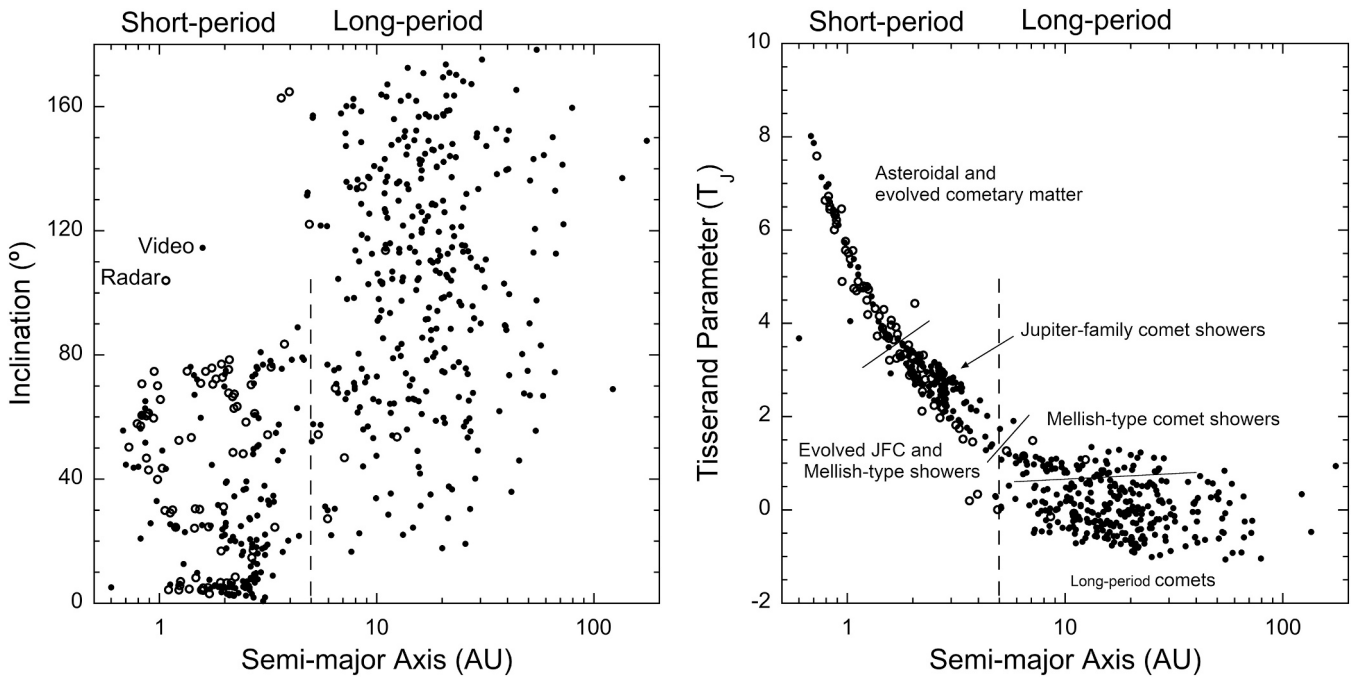

Fig. 8. A The median inclination of all video (•) and radar (o) detected meteor showers are plotted against the semi-major axis of the orbit. A dashed line gives the approximate distinction between short-period and long-period comet showers. B – The Tisserand parameter with respect to Jupiter for all meteor showers based on their median orbital elements. The meteoroid streams are dynamically evolved and traditional boundaries (< 1 for long period comets, 1-2 for Halley-type comets, 2–3 for Jupiter-family comets, and > 3 for asteroids) differ slightly from those of their parent bodies.

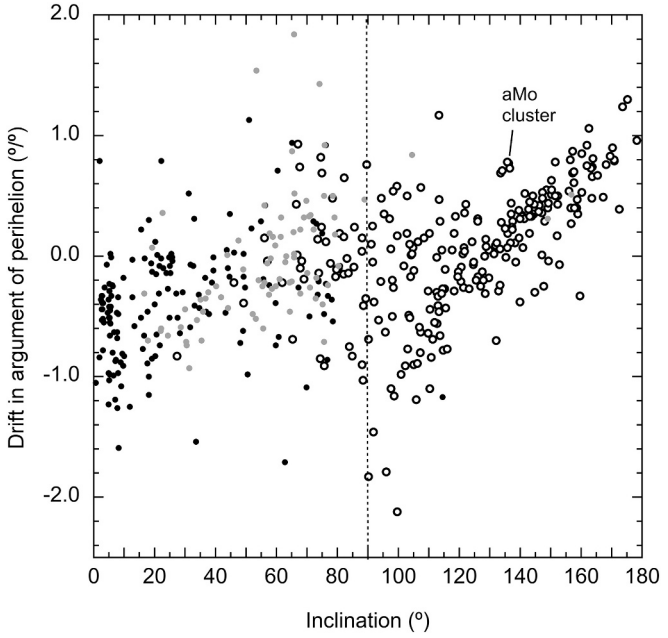

Fig. 9. The drift in argument of perihelion versus inclination for all showers. Long-period comet showers with $T_J < 0.64$ are shown as open circles and Mellish-type showers with $0.64 < T_J < 1.7$ as gray solid symbols. The remainder are Jupiter-family comet and primitive asteroid showers. A small grouping identified as "aMo cluster" contains the long-period alpha-Monocerotids shower (IAU#246). Dashed line marks the distinction between prograde (left) and retrograde (right) orbits.

90°) showers to the left and retrograde showers to the right.

As expected, the dispersions in argument of perihelion and inclination correlate with those in node. Each measure of dispersion includes an amount of measurement error. All video-detected showers combined have a median dispersion ±3.8° in node, ±3.8° in argument of perihelion, and 2.0° in inclination. The nodes are measured precisely, and measurement error in the dispersion of the node can be neglected. Most uncertainty in the nodal dispersion is from extracting the shower from the sporadic background. The median measurement error as determined from propagating Monte Carlo type error estimates in time, radiant and speed for individual meteors amounts to about ±0.5° in inclination and ± 0.7° in argument in perihelion (Jenniskens et al., 2011).

Dispersions in inclination (Fig. 10A) are low for Jupiter family comet showers in the anthelion and helion sources that have inclination <20°. Dispersions are high for toroidal sources that have inclinations in the range $20 < \imath < 90°$. Both trends could signify age, with Jupiter-family comet showers typically being dispersed rapidly by planetary perturbations, so most showers are young, while toroidal showers are dynamically evolved by Kozai cycles and tend to be old (e.g., Jenniskens, 2006). The dispersions do not correlate with the sine of the inclination of the orbit, for $20 < \imath < 160°$.

The dispersions in argument of perihelion (Fig. 10B) tend to be lower when $\omega \sim 0°$ and 180°, which is on account of geometry. Increased dispersion tends to move the meteoroids out of Earth's orbit so that each shower measures only a narrow range in ω.

As expected, the dispersion in node (Fig. 10C) does not correlate with the node itself. After correcting for attack angle, the dispersion is about half the dispersion in argument of perihelion for long-period comet showers, with no dependency on inclination $65° < \imath < 175°$. Among prograde Mellish-type showers (gray symbols in Fig. 9), most with $\imath < 65°$ have a dispersion in node about two times higher than the dispersion in argument of perihelion. The dispersion in node is about equal to the dispersion in inclination, except for $\imath < 20°$, where the dispersion in node is typically higher. The dispersion in inclination is about half the dispersion in argument of perihelion, except in the inclination range $20 < \imath < 65°$, where the dispersion is about equal.

Neglecting a possible factor of two weight for inclination, we defined a combined dispersion simply as:

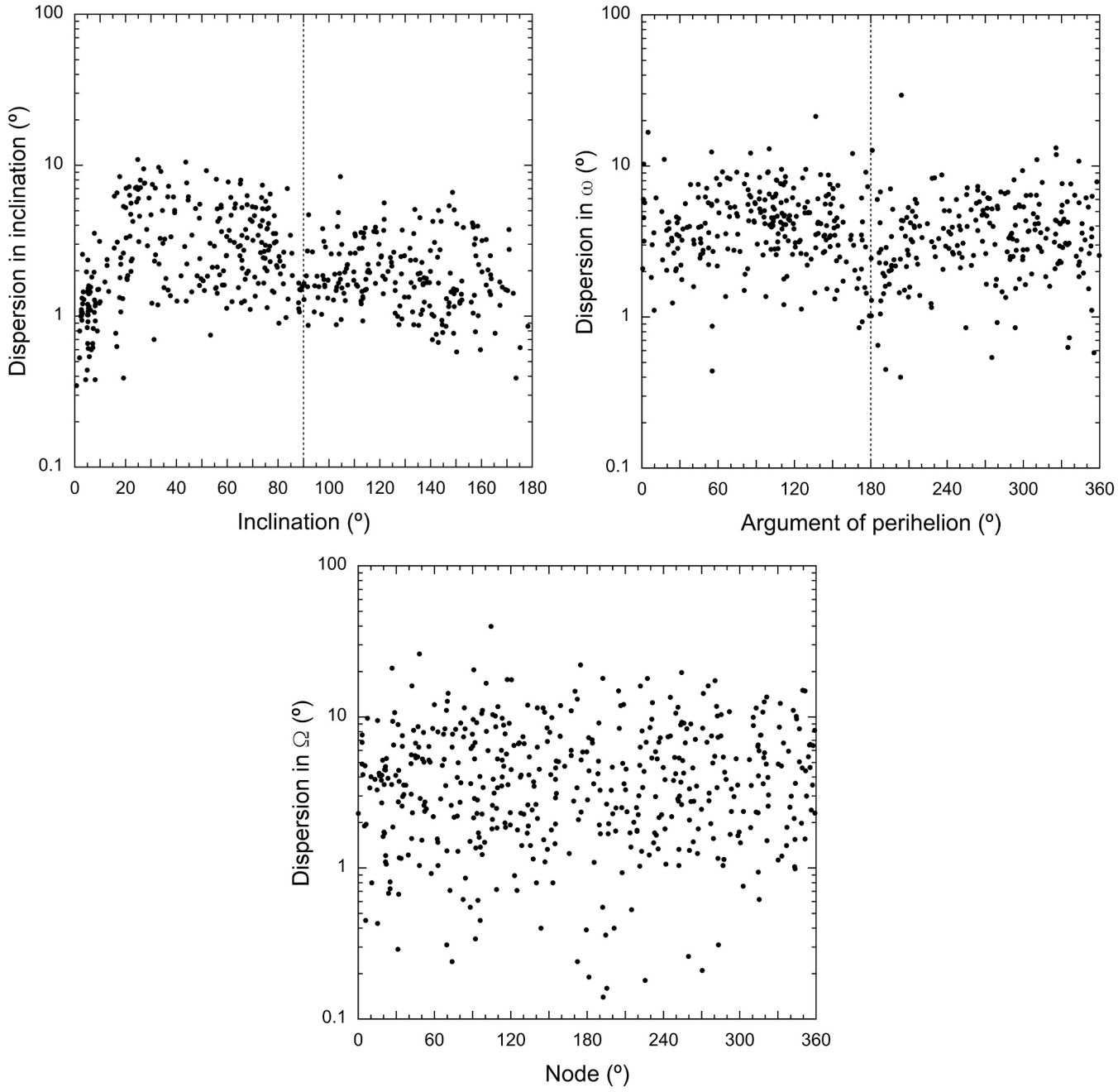

Fig. 10. A The dispersion of inclination as a function of inclination, with prograde showers on the left side of the dashed line and retrograde showers on the right side. B – As Fig. 10A for the dispersion of the argument of perihelion as a function of the argument of perihelion. C – As Fig. 10A, for the dispersion of node as a function of node.

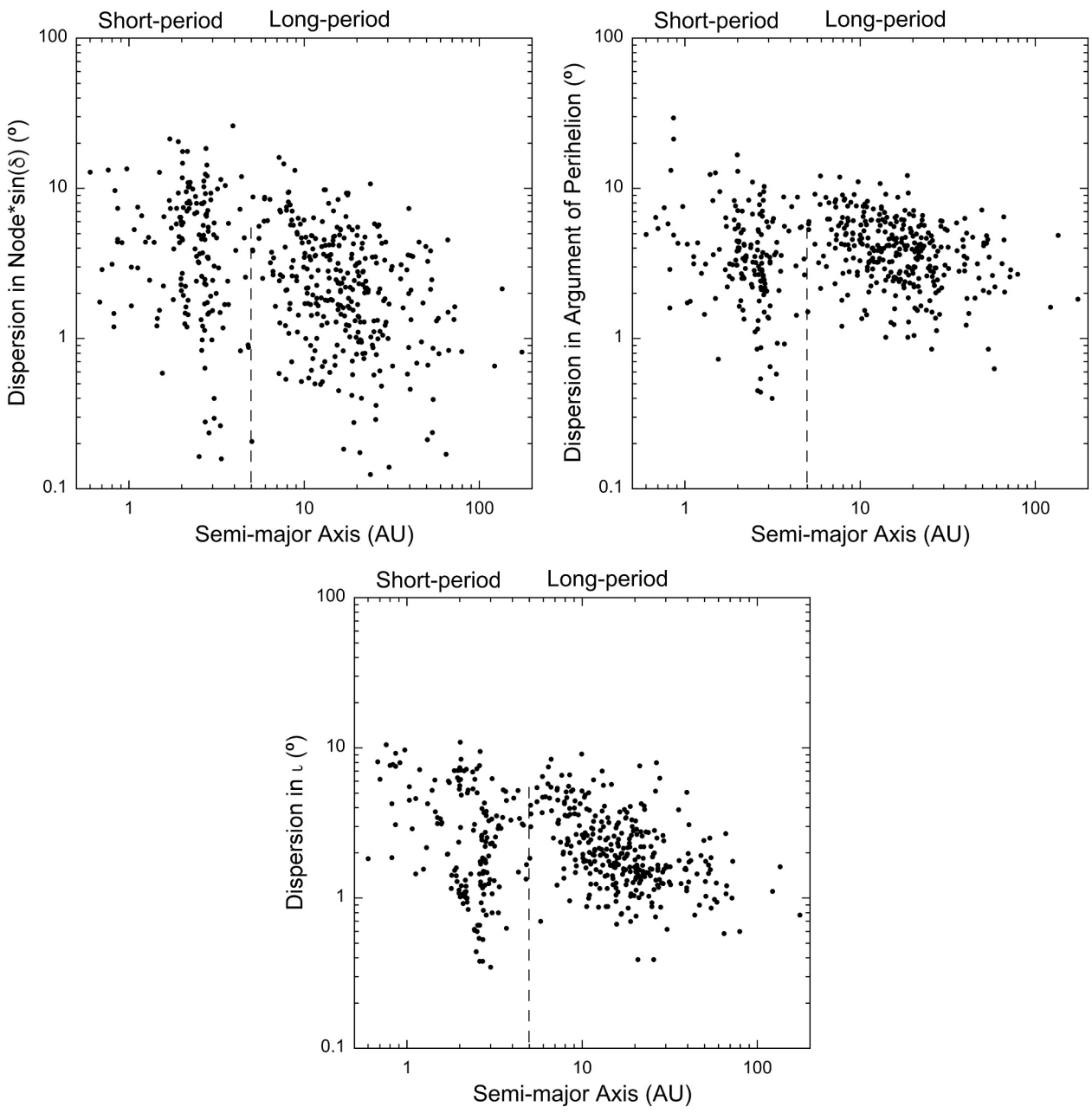

Fig. 11. A – The dispersion in node, corrected for attack angle δ, for each shower is shown versus semi-major axis in the manner of Fig. 8A. B – Same as Fig. 11A, for dispersion in argument of perihelion (ω). C – Same as Fig. 11A, for dispersion in inclination (*ι*).

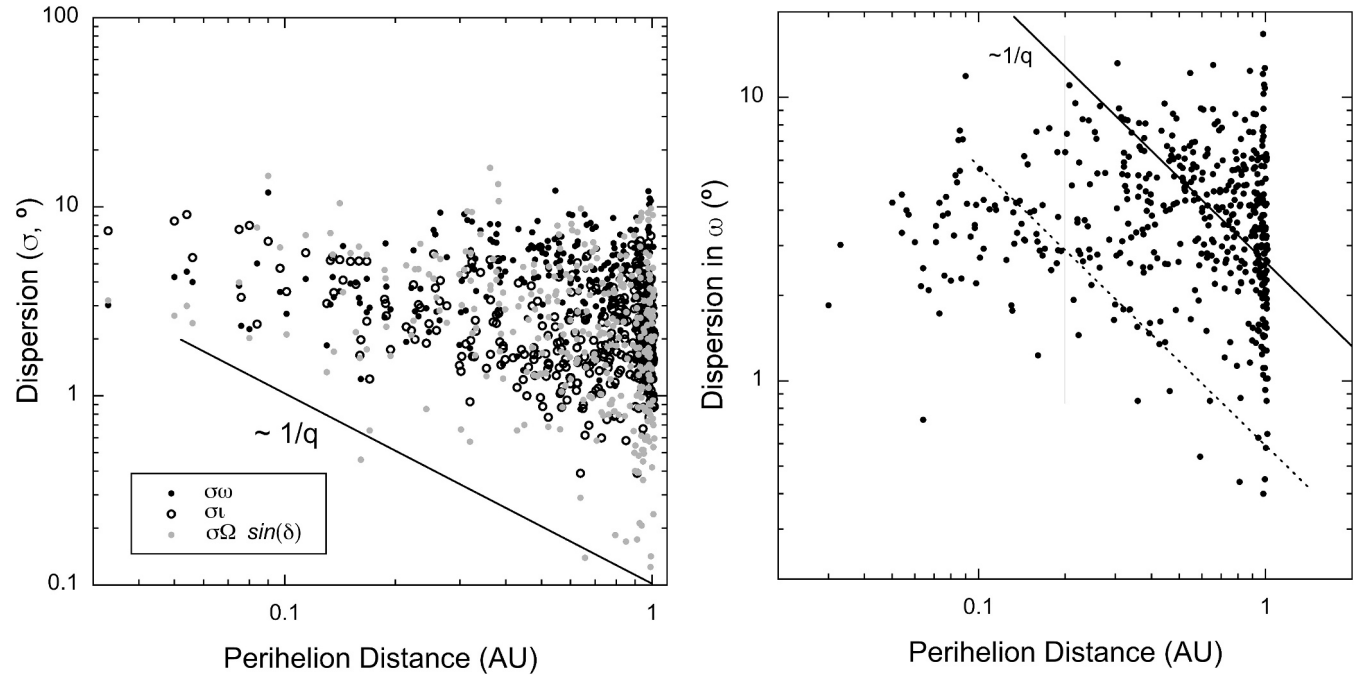

Fig. 12. A – Dependence of the three angular dispersions on the perihelion distance (q) of the orbit for all long-period and Mellish-type showers. The solid line shows the expected slope of a 1/q dependence. B – As Fig. 12A, but for all meteor showers. The slanted lines are proportional to 1/q and are scaled to match older showers (solid line) and young showers (dashed line).

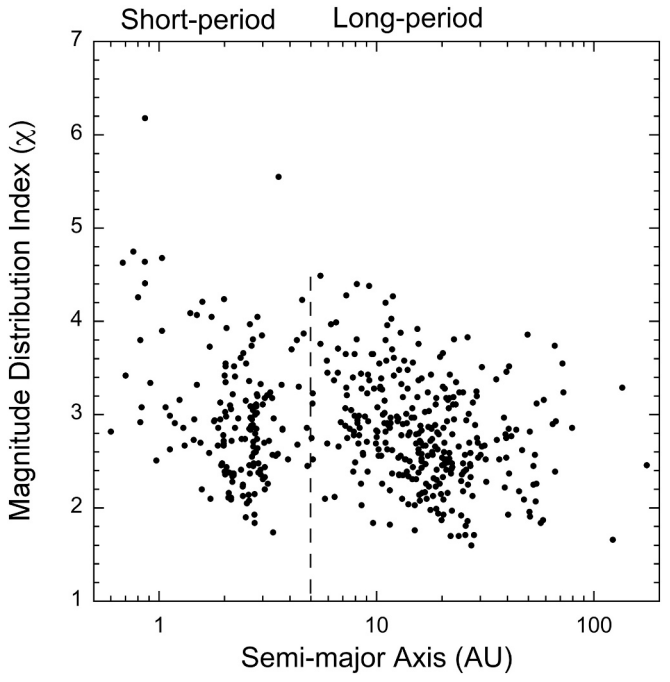

Fig. 13. Same as Fig. 11A, for the value of the magnitude size distribution index (χ) of each shower.

$$\sigma_{tot} = \sqrt{(\sigma\iota^2 - 0.5^2) + (\sigma\omega^2 - 0.7^2) + (\sigma\Omega sin(\delta_v))^2} \quad (12)$$

Fig. 11A–C compare the dispersions for different comet types. The dispersion in node (Fig. 11A) tends to increase for shorter period orbits, but no longer for a < 2 AU. For long-period comets, the dispersion in inclination also tends to increase with decreasing semi-major axis. The dispersion in inclination is clustered among short-period showers, reflecting the presence of shower complexes (e.g., Taurid Complex).

Finally, we examined the dependence of dispersions on the perihelion distance, assuming all values of perihelion distance sample the same range of shower ages. Fig. 12A shows the dispersions for all long-period and Mellish-type showers. The lower limit of dispersion follows a 1/q dependence as indicated by the slope of the solid line. The showers near this lower limit have the lowest dispersions and are the young showers in each bin of q. The population of older showers may follow a similar trend, but only until reaching a maximum dispersion of about 10°. There is likely an upper limit to the dispersions based on what showers can still be separated from the sporadic background. The most dispersed showers have σΩ * sin (δ) ~ 20°. Hence, this upper limit could be an observational limitation to detecting very dispersed showers in the apex source, or it could be an effect of age, where the meteoroids are lost from the stream when reaching this limit.

Fig. 12B plots the dispersion of the argument of perihelion for all showers (including Jupiter-family comet showers) as a function of perihelion distance on a log-log scale. Solid and dashed lines are proportional to ~1/q. For q ~ 1 AU, there is a full range of dispersions, but for q < 0.2 AU there are only small values. We interpret this to mean that showers with q < 0.2 AU do not sample the same range in age and are mostly young showers.

3.3. Magnitude size distribution index

The magnitude size distributions show much the same patterns with semi-major axis as seen in the orbital elements: broader (older) streams have on average higher magnitude size distribution indices (Fig. 13).

Magnitude size distributions are measured independently from the stream dispersions. Because radiation forcing plays such a small role, the main cause of the dispersions in orbital elements is gravitational perturbations, which are independent of mass in the size range considered here.

Showers with high magnitude distribution index tend to be more dispersed (Fig. 14). The correlation coefficients are not high, however. Looking at individual orbital element dispersions, we have for σω a correlation coefficient $r = 0.41$, for σι: $r = 0.46$, and σΩ: $r = 0.32$. Restricting the sample to only long-period comet showers (shown in

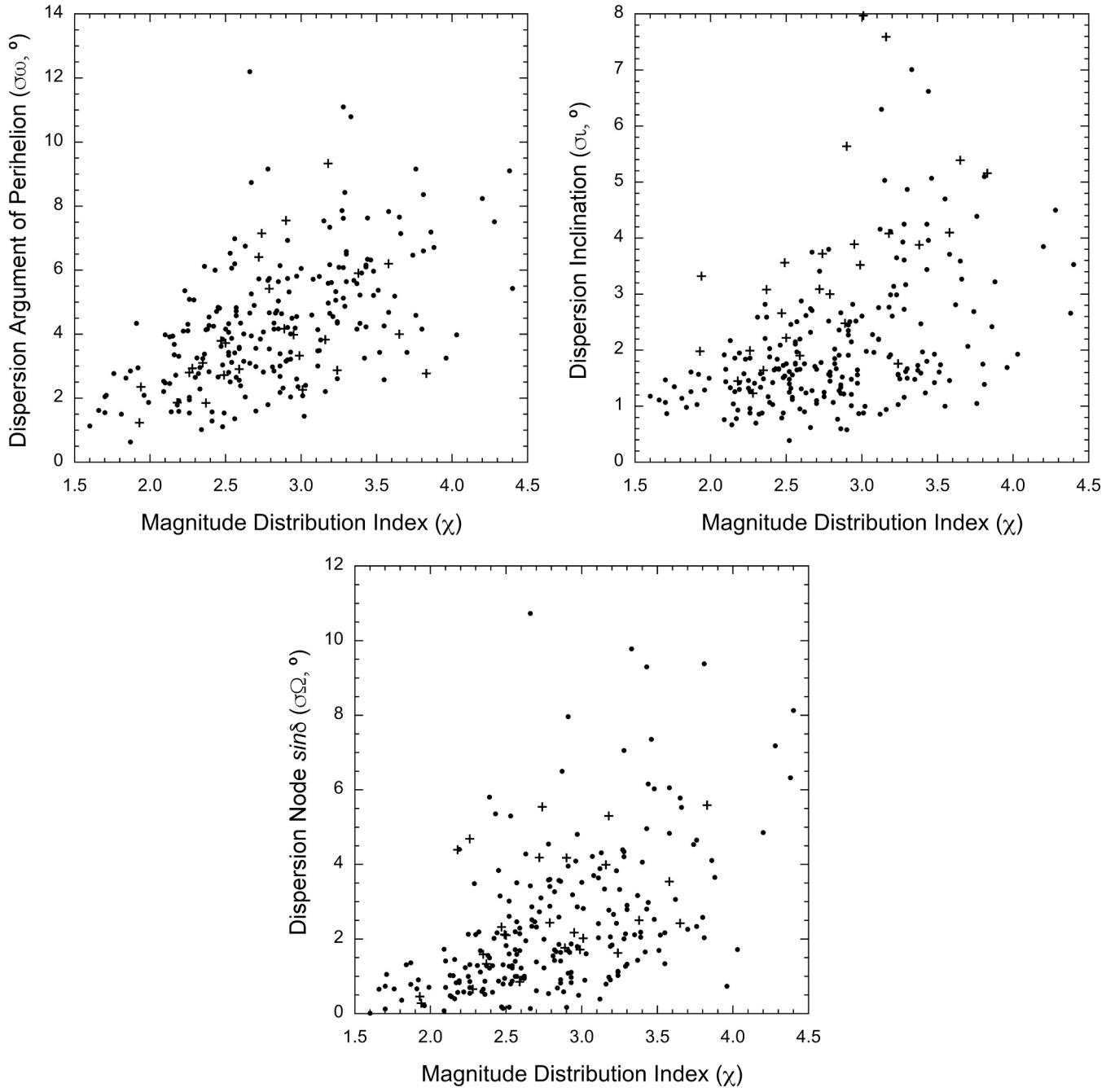

Fig. 14. A – The observed dispersion in argument of perihelion is shown as a function of the magnitude distribution index for long-period comet showers. Solid points are showers with perihelion distance $q \geq 0.3$ AU, while crosses are those with $q < 0.3$ AU. B – As Fig. 14A, for the dispersion in inclination. C – As Fig. 14A, for the dispersion node corrected for attack angle.

Table 2
Correlations coefficients (r) in bins of perihelion distance (q) of shower dispersions versus magnitude distribution index for long-period comet showers with $20 < \iota < 160°$.

q (AU)	*r_ι*	*r_ω*	*r_Node*
0.05	0.079	0.132	0.165
0.15	0.378	0.096	0.391
0.25	0.847	0.325	0.503
0.35	0.415	0.475	0.330
0.45	0.401	0.700	0.669
0.55	0.583	0.601	0.187
0.65	0.558	0.672	0.489
0.75	0.531	0.397	0.269
0.85	0.545	0.654	0.503
0.95	0.433	0.543	0.292
1.007	0.024	0.216	0.291

Fig. 14A–C) does not change this picture: for σω: $r = 0.55$ (Fig. 14A), σι: $r = 0.48$ (Fig. 14B), σΩ: $r = 0.51$ (Fig. 14C). Either showers start out with different magnitude distribution index, they disperse at different rates depending on orbital elements, or the larger particles are lost at different rates depending on orbital elements or physical properties. Likely, all these issues play a role.

Checking to see if the dispersion is affected by perihelion distance (shown schematically as two groups of different symbols in Fig. 14A–C), we first excluded the low prograde $\iota < 20°$ and retrograde $\iota > 160°$ inclinations. Then, calculating correlation coefficients in steps of 0.1 AU in q shows that highest correlation coefficients for $20 < \iota < 160°$ are for $0.20 < q < 0.90$ AU, with σω: r = 0.55, σι: r = 0.55, σΩ: $r = 0.42$; and lower values for $q < 0.20$ AU and $q > 0.90$ AU (Table 2).

3.4. Light curve shape parameter

Fig. 15 shows the light curve shape parameter F values for the fluffy type Ia–II shower component (Fig. 15A) and the dense shower components IIb–IV (Fig. 15B), with symbols indicating shower type as in Fig. 6. Values for the Ia–II component mostly scatter between 0.45 and 0.76 and appear to be slightly higher on average for Jupiter-family comet streams (Fig. 15A). The difference is less clear for the dense shower component (Fig. 15B), where both comet types show the same range of F.

Among the fluffy type Ia–II shower components, long-period comets have two types of materials, with a group at relative high F ~ 0.65 (mostly type Ib showers) and a group at F ~ 0.53 (mostly type I showers). Going from high median values of semi-major axis a ~ 60 AU to low values a ~ 8 AU in this population shows initially a preponderance of type I showers, but then a preponderance of type Ib showers.

Showers with small perihelion distance tend to be type II showers, not type I. Among the type I showers, there is no clear dependence of F value with perihelion distance, except that there are significantly few low values of F for $q < 0.3$ AU (Fig. 16).

3.5. Meteoroid density

The median meteoroid densities calculated are plotted in Fig. 17. Long-period comet showers tend to have lower densities than Jupiter-family comet showers, but there are exceptions. Notably the Draconids of comet 21P/Giacobini-Zinner have the lower density of 0.3 g/cm^3 typical of long-period comet showers. The long-period comet shower group also has some showers with properties more similar to those of Jupiter family comets.

Low density meteoroids do tend to have a lower F-value (Fig. 18), as expected if low density meteoroids fragment more easily.

Meteoroids in orbits with low q tend to have higher densities (Fig. 19). For $q < 0.2$ AU, the type II showers dominate. The type II showers in Fig. 19 that have q ~ 0.3 AU are members of the Taurid shower Complex. Overall, there is a 1/q dependence among Type I showers (open circles and gray dots).

3.6. Fraction of dense (low beginning height) meteors over total

Fig. 20A shows the fraction of dense over total meteoroids (f_d) as a function of semi-major axis to show the different comet shower populations separately. Fig. 20B shows this ratio as a function of perihelion distance.

We find that for the long-period comet population, the fraction of dense meteoroids in the population increases when the shower evolves

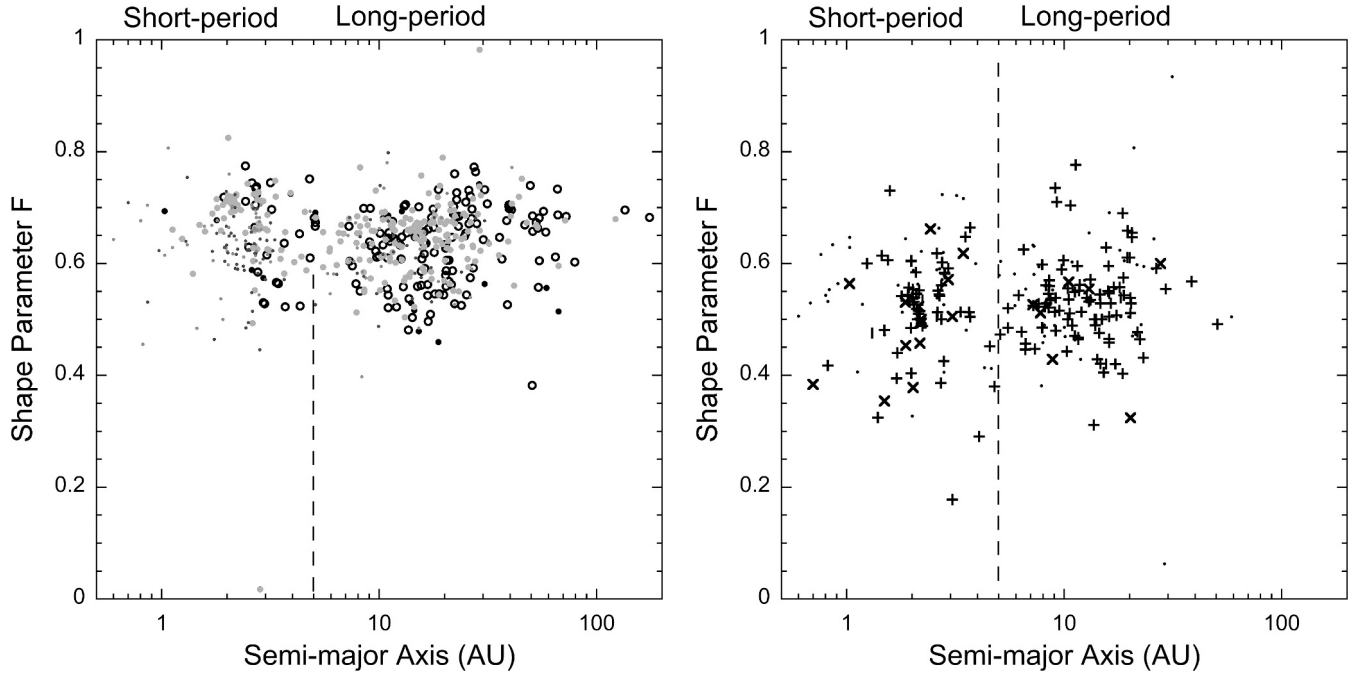

Fig. 15. A – The value of the light curve shape parameter (F) for fluffy shower components of type Ia – II, with each type shown with the symbols of Fig. 6. B – As Fig. 15A, for the shower components of type IIb – IV, with symbols as in Fig. 6.

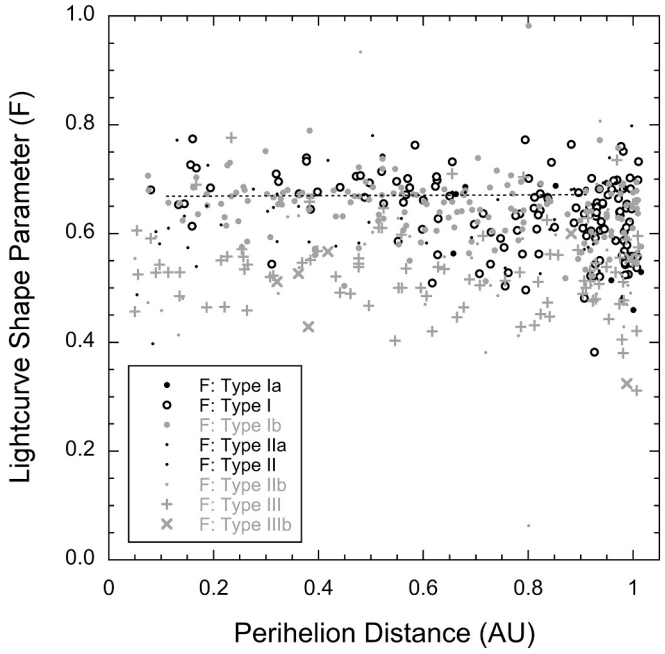

Fig. 16. The lightcurve shape parameter (F) of all showers as a function of the current perihelion distance of the orbit. Symbols as in Fig. 6.

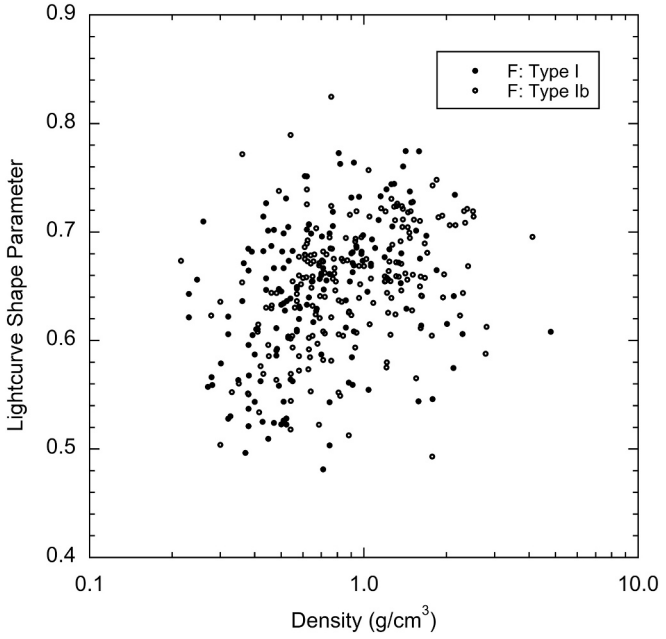

Fig. 18. The lightcurve shape parameter F-values as a function of meteoroid density for two "fluffy" types I and Ib (core of the band I).

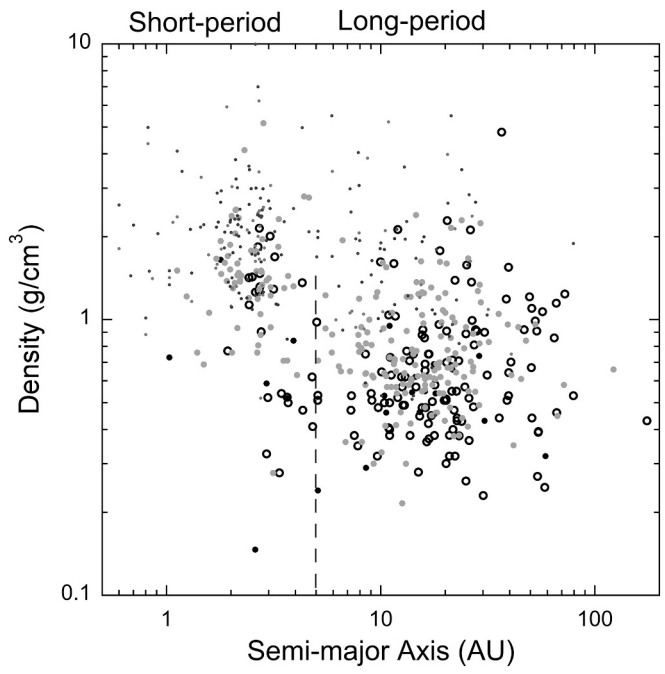

Fig. 17. Same as Fig. 11A, for the meteoroid density (ρ), with symbols as in Fig. 6.

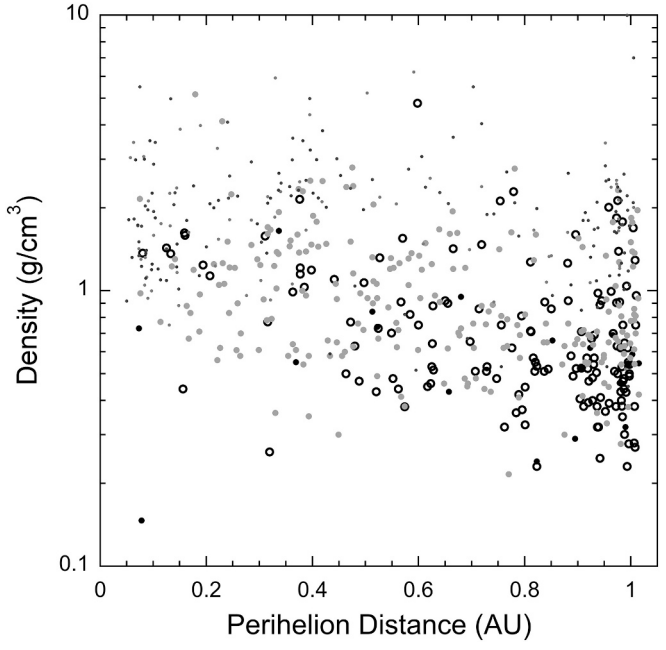

Fig. 19. The density of meteoroids in all showers as a function of perihelion distance. Symbols as in Fig. 6.

(with age) to lower semi-major axis. Low-fractions of dense material are found in some of the Jupiter-family comet showers. High fractions, up to 100%, are found in low-q showers, with q < 0.2–0.3 AU.

4. Dispersions and physical parameters as a function of age

Meteoroid streams are expected to disperse over time. In order to quantify these changes, and catalog the changes in the size distribution index and meteoroid physical properties over time, the ages of observed meteoroid streams need to be determined.

Numerous published dynamical models of meteoroid streams attempt to do just that, but show a lot of discrepancies between studies. A summary of that literature is provided in Jenniskens (2006, 2023). These studies require that the parent body, if known, be integrated back in time, then a cloud of meteoroids be integrated forward in time. The backward integration of the parent comet is not unique, and a subsequent forward integration doesn't necessarily bring the comet back to its observed orbit. In addition to the random nature of planetary perturbations, there are the unknown non-gravitational perturbations on the comet orbit. Finally, the comet activity may not be constant over time. Indeed, fragmentation is a dominant mechanism of meteoroid stream

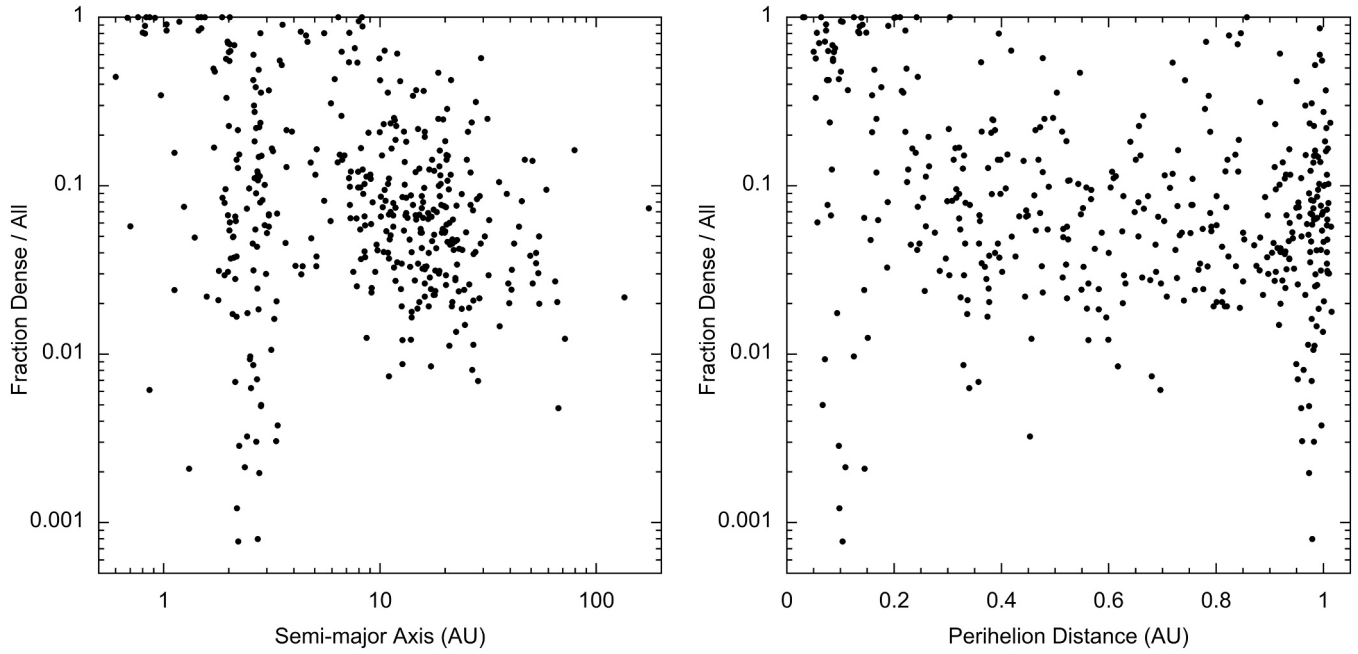

Fig. 20. A – The fraction of dense particles (types IIb–IV) relative to the total for all showers. B – As Fig. 20A, but now plotted as a function of perihelion distance q.

Table 3
Perseid meteor shower components, with orbital elements perihelion distance (q), inclination (ι), dispersion in inclination, argument of perihelion (ω) and Node (Ω), the magnitude distribution index (χ), the age of the stream and the literature reference for the age information.

#	Component	q (AU)	i (°)	$\sigma\iota$ (°)	$\sigma\omega$ (°)	$\sigma\Omega$ (°)	χ	Age (y)	Ref
7	1862-dust trail $\lambda_o \sim 140°$	0.960	113.39	0.23	0.58	0.040	1.72 ± 0.07	~130	[1,2]
7	1610-dust trail $\lambda_o \sim 140°$	0.960	113.39	0.23	0.58	0.040	1.96 ± 0.07	~381	[1,2]
7	1079-dust trail $\lambda_o \sim 140°$	0.960	113.39	0.23	0.58	0.040	2.12 ± 0.07	~939	[1,2]
7	Filament $\lambda_o \sim 140°$	0.959	113.42	0.24	0.61	0.048	1.99 ± 0.13	390–1500	[1,2]
7	Annual Peak $138 < \lambda_o < 142°$	0.949	113.0	2.85	6.15	0.90	2.36 ± 0.03	3000–20,000	[4,5,6]
7	July-Tail $125 < \lambda_o < 130°$	0.956	111.6	4.00	5.84	1.39	2.83 ± 0.06	27,000–40,000	[3,4,6]
7	July-Tail $\lambda_o \sim 117.5°$	1.002	109.7	4.11	5.82	2.17	3.09 ± 0.06	100,000–160,000	[1,6]

Notes: References to age estimates: [1] Jenniskens (2006); [2] Jenniskens et al. (1998); [3] Hamid, 1954; [4] Jones & Brown (1998); [5] Harris et al., (1995); [6] Jenniskens (2023).

formation among short-period comets (Jenniskens, 2006).

Here, we will first discuss the cases of Perseids and Taurids, from which Earth samples different parts of the stream complex, and then expand on the population of long-period comets, which are least affected by resonances and close encounters with the main planets.

4.1. The Perseid shower components of comet 109P/swift-Tuttle

Perseid shower parent comet 109P/Swift-Tuttle has a large ~26 km nucleus and passes relatively close to Earth's orbit. Due to its large size, the comet orbit is unaffected by non-gravitational forces and its past orbit can be traced comparatively reliably (Yau et al., 1993). It is not known, however, what was the activity of the comet in the past.

Halley-type showers such as the Perseids of comet 109P/Swift-Tuttle move in orbits that resonate with the orbit of Jupiter, or they librate about such resonances, so that the stream is relatively little perturbed from close encounters with Jupiter itself. That can also limit the rate of dispersion. The number of meteoroids in these confined configurations can build up over time, making these some of the richest meteoroid streams. The comet orbit itself may have evolved away from the part of the stream that is now encountered at Earth, but that is not the case for the Perseids.

Recent comet ejecta of 109P/Swift-Tuttle encountered at Earth tend to be rich in bright meteors, with dust thought to have ejected during the previous 1862 CE return having a low magnitude distribution index of $\chi \sim 1.72 \pm 0.07$ (e.g., Brown and Jones, 1998; Jenniskens, 2006, 2023). Some other dust trail encounters have also been identified (Table 3), but those identifications are uncertain because of the similarity in width to the Filament component. The measured magnitude distribution index is also uncertain due to the strong annual shower background.

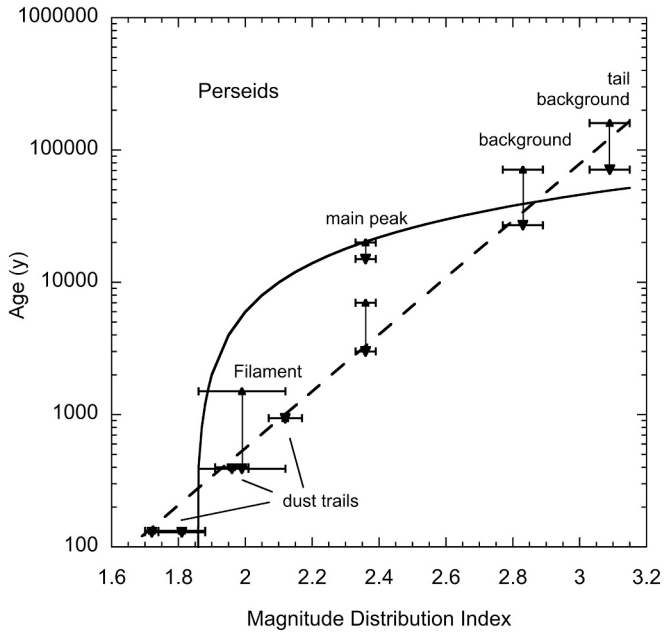

Fig. 21. The magnitude distribution index of Perseids for different age components. The solid line assumes that the magnitude distribution index increases proportional to age, while the dashed line shows a dependence proportional to the logarithm of age.

Other Perseid meteor shower outbursts appear to be accumulated dust from multiple returns forming what was called a "Filament" (Jenniskens et al., 1998). These also tend to have low magnitude distribution index. Measured values varied from $\chi \sim 1.86 \pm 0.14$ in 1991, 2.12 ± 0.15 in 1992, 2.02 ± 0.04 in 1993, and 1.9 ± 0.2 in 1994 (Jenniskens, 2006) (Table 3). The Filament has about twice the dispersion in node as the 1-revolution 1862 dust trail. The age is uncertain, presumably representing a number of comet orbits.

The peak of the annual meteor shower contains relatively more faint meteors ($\chi \sim 2.36 \pm 0.03$) and is significantly wider. The main peak is due to dust particles produced in the last 5000 years according to Harris et al. (1995), while Brown and Jones (1998) suggest the meteoroids accumulated over a 15,000–20,000 year period.

The Perseid main activity peak has a broad background component with an early onset in July. The Perseid maximum has $\sigma\Omega < \sigma\omega$, while this background has $\sigma\Omega \sim \sigma\omega$. The dust has a magnitude distribution index of $\chi = 2.83 \pm 0.06$. Harris et al. (1995) showed that this component is now understood to be debris located just outside Earth's orbit ejected in the past, when precession of the node had not yet advanced into August. Dust in the longest period orbits took more time to return and the node precessed less quickly over the years (Jenniskens, 2006). From the calculated rate of precession of the comet orbit, at the moment $+0.0002029^\circ$/year (Yau et al., 1993), the age of dust at 130° solar longitude is $\leq$47,000 y, at 125° $\leq$ 71,000 y. An early estimate put the age of the extended stream at about 40,000 y (Hamid, 1954).

The comet was last near Jupiter's orbit ~160,000 y ago, when it may have been captured (Harris et al., 1995). The magnitude distribution index is $\chi = 3.09 \pm 0.06$ for $\lambda_o = 117.5^\circ$, when the meteoroids were ejected at least 108,000 y ago.

All data combined (Table 3) suggests that the magnitude distribution index ($\chi = N(m+1)/N(m)$) changes logarithmically with age (Fig. 21, dashed line):

$$\text{Age (y)} = 0.028\, exp(4.95\chi) \quad (13)$$

On the other hand, if we accept the Brown and Jones (1998) age of the main peak as opposed to that of Harris et al. (1995), then a linear fit to the age would also satisfy the data. The solid line in Fig. 21 is the relationship (with q the perihelion distance, see below):

$$\text{Age (y)} = 40,000\sqrt{q}\,(\chi - 1.85) \quad (14)$$

These Perseids range from +4 to −5 magnitude, corresponding to masses of about 0.0008 to 3 g, centered on 0.03 g (+0 magnitude). Because the magnitude distribution index is increasing in time, that means that the 0.03-g grains disappear faster than small 0.0008 g grains. If the relationship is logarithmic, remaining dust grains would need to live exponentially longer over time.

4.2. The Taurid complex of comet 2P/Encke

There are not many other meteor showers that have components of a variety of ages for which the ages were estimated. The most interesting short-period case is that of the Taurid Complex showers of comet 2P/Encke. The Complex consists of night-time northern and southern branches for the stream on the way towards the Sun (in anthelion source), and day-time northern and southern branches on the way out (in helion source). The night-time branches have been studied best with video cameras and there appear to be a number of distinct components that cause the radiant of the stream to jump from component to

Table 4
As Table 3, for the Taurid Complex meteor shower components.

#	Component	q (AU)	i (°)	σι (°)	σω (°)	σΩ (°)	χ	Source	Age(y)	Src
628	s-Taurids *	0.372	5.3	1.02	3.42	8.16	2.11 ± 0.12	2015 TX24	2,6-5200	[1]
17	Northern Taurids	0.360	2.9	1.32	5.31	18.0	2.72 ± 0.06	2P	10,500	[2]
173	Daytime β-Taurids	0.230	3.3	1.45	8.37	10.4	2.96 ± 0.73	2P	7–14,000	[2]
2	Southern Taurids	0.333	5.5	1.59	6.18	21.1	2.95 ± 0.13	2P	14,500	[2]
172	Daytime ζ-Perseids	0.330	5.5	1.41	8.31	9.64	3.13 ± 0.14	2P	16,000	[2]
624	xi-Arietids	0.337	5.6	1.16	2.60	1.87	2.93 ± 0.37	2011 UD	4–8000	[3]
625	lambda-Taurids	0.464	5.0	1.02	4.03	2.74	2.36 ± 0.10	2005 UR	5200	[3]
626	lambda-Cetids	0.359	5.4	1.13	4.47	2.57	2.67 ± 0.10	2007 RU17	16,000	[3]
627	nu-Piscids	0.316	5.3	1.53	3.11	7.62	2.86 ± 0.18	2010 RV3	4000	[3]
629	A2 Taurids	0.396	2.7	1.03	2.52	1.65	2.11 ± 0.05	2014 NK52		[3]
630	tau-Arietids	0.336	3.0	1.05	1.79	1.29	2.11 ± 0.05	2005 TF50	2–5200	[3]
631	delta-Arietids	0.296	3.1	1.21	1.64	2.01	2.44 ± 0.16	2P	1–2000	[3]
632	November eta-Taurids	0.357	2.8	1.07	1.55	1.22	2.09 ± 0.14	2004 TG10	4–8000	[3]
633	p-Taurids	0.419	2.6	1.07	2.71	2.26	2.38 ± 0.02	2012 UR158		[3]
634	tau-Taurids	0.426	2.6	1.11	1.35	1.82	2.37 ± 0.08	2003 UL3	16,000	[3]
635	A1-Taurids	0.374	2.7	1.01	1.52	1.47	2.28 ± 0.09	2019 UN12	8000	[3]
637	f-Taurids	0.401	5.3	1.08	3.83	2.32	2.69 ± 0.14	2010 TU149	8–16,000	[3]
25	North. Oct. δ-Arietids	0.316	3.6	1.29	5.37	4.94	2.46 ± 0.05			[3]
28	South. Oct. δ-Arietids	0.285	5.8	1.42	3.15	4.12	2.94 ± 0.11		8000	[3]
286	omega-Taurids	0.515	5.2	0.92	5.07	1.48	2.16 ± 0.02			[3]

Notes: *) Breakup of 2015 TX24 from 2P;[1] Egal et al. (2021); [2] Egal A., et al. (2022a,b); [3] Tomko and Neslusan (2019).

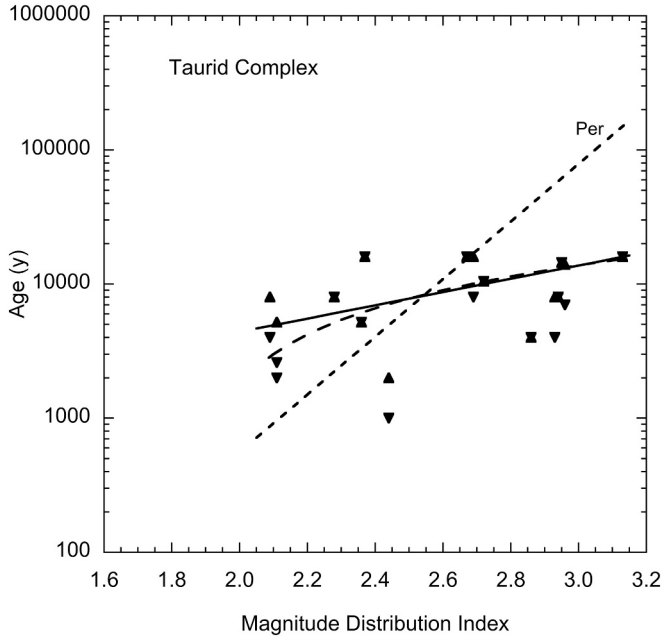

Fig. 22. The magnitude distribution index of Taurid Complex showers for different age components. The solid line is an exponential fit to the data, the dashed line a linear fit. The dashed line labeled "Per" is the dashed line in Fig. 21.

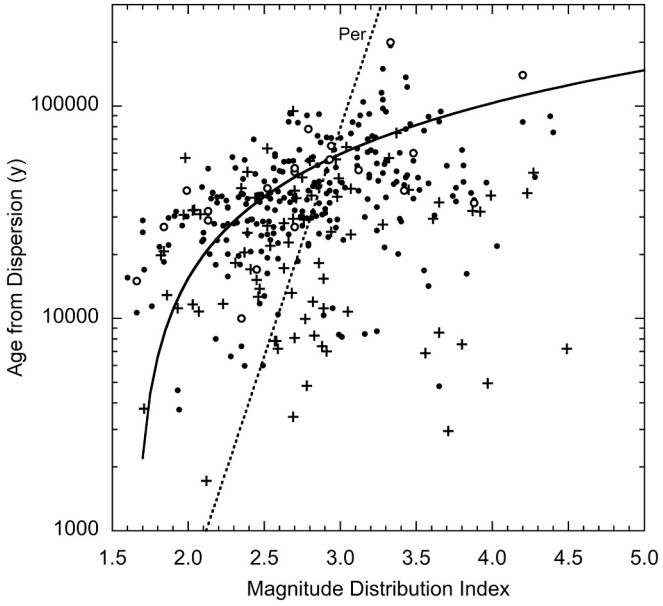

Fig. 23. The shower age derived from dispersions as a function of the magnitude distribution index for all long-period comets. Ages derived from modeling are shown as open circles, while the ages derived from a generalized equation proportional to dispersion are shown for long-period comets (•) and Mellish-type comets (+). The solid line has the magnitude distribution index increase proportional to age, while the dashed line labeled "Per" is the exponential-fit dashed line of Fig. 21.

component (Jenniskens et al., 2016a; Jenniskens, 2023). These components have individual parent objects associated with them, all with orbits that could make these fragments of comet 2P/Encke. Table 4 gives an overview.

2P/Encke moves in an orbit decoupled from Jupiter. Showers in the Taurid Complex evolve gradually by rotating the nodal line over a timescale of about 5000 y (Hamid, 1954). The streams are only observed when one of the nodes evolves into Earth's path. In addition, the longitude of perihelion precesses, which changes the node over time. If showers are relatively short-lived, the Complex as a whole will be distributed as much as the parent bodies are.

The case of the Taurids was discussed in Jenniskens et al. (2016a). The key observation was that the Taurids do not strictly have twin showers. While the Northern and Southern Taurids are considered twin streams, they do not have the same nodal distribution as would have been expected from rotation of the nodal line. Individual components of the Southern Taurids do not have a counter part in the Northern Taurids.

That is most obvious for shower 628, the s-Taurids, which cause meteor outbursts every 3 years from the Southern Taurid component, with no similar component in the Northern Taurids, likely due to dust trapped in the 7:2 mean motion resonance (Asher and Izumi, 1998; Spurny et al., 2017). The likely parent body is asteroid 2015 TX_{24}, which broke from comet 2P/Encke about 5200 years ago (Devillepoix et al., 2019). The stream may have that same age if most of the dust is from that breakup, or half that value, if ongoing activity from 2015 TX_{24} is responsible. Note that for this low-inclined Jupiter-family shower, there is a significant dispersion in both the node (Ω) and the argument of perihelion (ω), despite the young age of the stream, but the longitude of perihelion (ω+Ω) is nearly constant.

Table 5
As Table 3, for the modeled long-period comet meteor showers.

#	Component	q (AU)	i (°)	σι (°)	σω (°)	σΩ (°)	χ	Source	Age (y)
6	April Lyrids	0.920	79.4	2.17	3.92	1.17	2.13 ± 0.03	C/1861 G1	29,000
130	delta-Mensids	0.963	59.6	2.51	2.96	5.88	2.70 ± 0.06	C/1804 E1	51,000
145	eta-Lyrids	1.000	74.4	1.66	1.60	1.53	2.70 ± 0.04	C/1983 H1	49,000
206	Aurigids	0.677	148.0	1.45	5.74	7.43	2.79 ± 0.02	C/1911 N1	78,000
331	alpha-Hydrids	0.314	61.5	4.67	8.52	10.54	2.94 ± 0.07		65,000
410	delta-Piscids	0.920	178.3	0.86	3.49	2.15	3.12 ± 0.14		50,000
427	February eta-Draconids	0.971	55.4	1.53	2.02	0.62	2.45 ± 0.20		17,000
458	June epsilon-Cygnids	0.920	95.7	1.33	2.46	0.62	2.13 ± 0.05		32,000
510	June rho-Cygnids	1.007	88.5	1.50	1.87	0.86	1.99 ± 0.05		40,000
517	April lambda-Ophiuchids	0.303	110.8	1.62	4.06	4.09	2.52 ± 0.28		41,000
519	beta-Aquariids	0.919	156.0	1.24	3.25	5.63	3.42 ± 0.15		40,000
569	omicron-Hydrids	0.680	114.3	3.85	8.24	7.41	4.20 ± 0.36		140,000
571	26-Bootids	0.497	83.1	0.98	2.63	1.55	1.84 ± 0.11		27,000
647	beta-Comae Berenicids	0.640	22.1	1.98	3.79	9.83	2.35 ± 0.09		10,000
681	omicron-Aquariids	0.363	161.9	3.22	6.71	6.78	3.88 ± 0.17		35,000
798	August Caelids	0.994	83.6	7.01	10.79	11.47	3.33 ± 0.14		200,000
822	Nu Taurids	0.562	135.9	1.93	5.21	10.77	3.48 ± 0.27		60,000
828	31 Pegasids	0.247	49.2	2.41	2.18	4.76	2.70 ± 0.45		27,000
839	phi-Serpentids	0.429	69.0	1.11	1.62	0.73	1.66 ± 0.55		15,000
1047	gamma-Crucids	0.929	102.8	1.48	3.44	1.54	2.93 ± 0.19		56,000

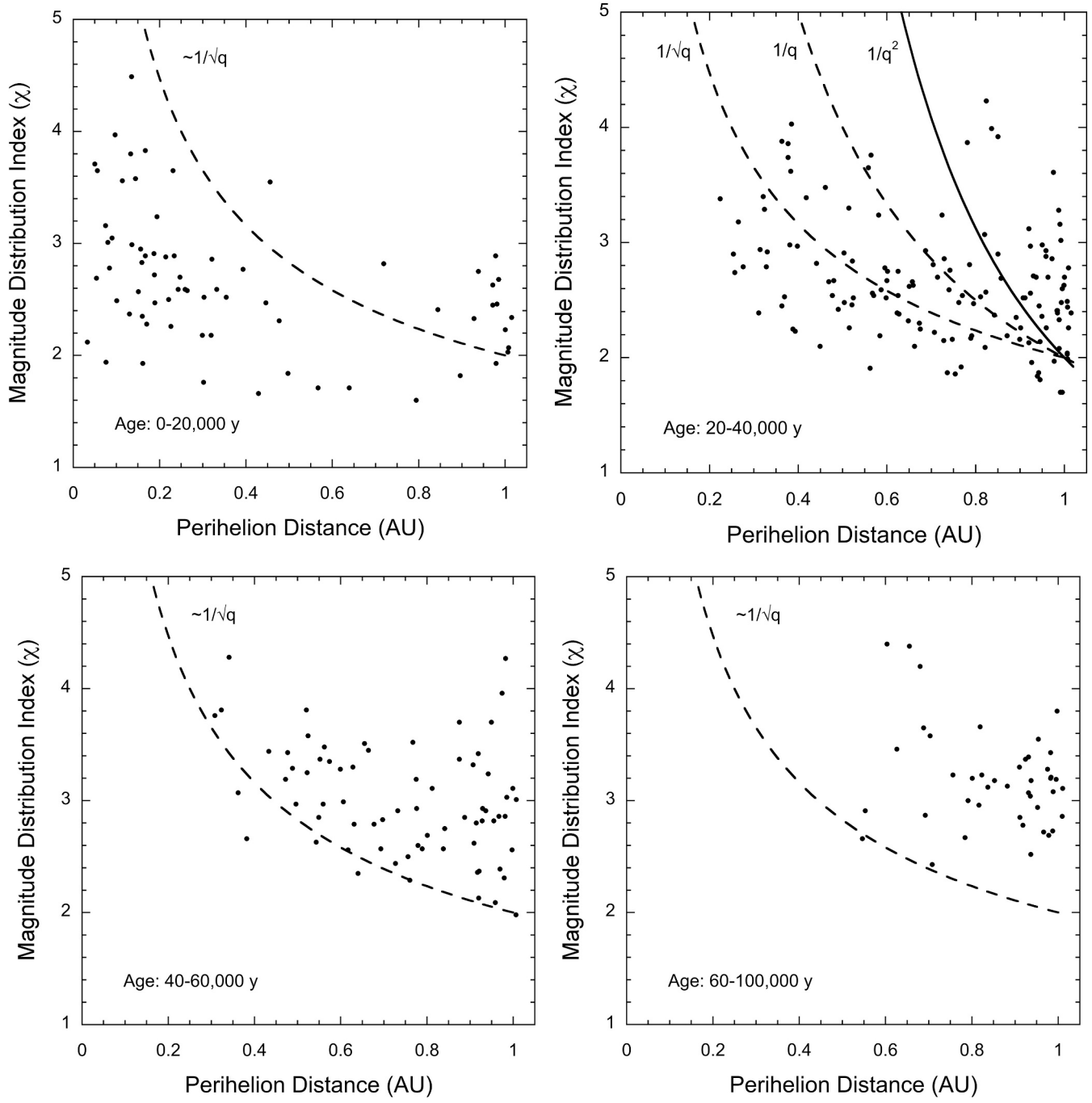

Fig. 24. A – Magnitude distribution index as a function of perihelion distance only for young showers of 0–20,000 y age. The dashed line is proportional to $1/\sqrt{q}$. B – As Fig. 24A, for showers of 20–40,000 y age. The lower dashed line is that of Fig. 24A. Two other lines show the steeper dependence expected of $1/q$ and $1/q^2$. C – As Fig. 24A, for old showers of 40–60,000 y age. The dashed line is that of Fig. 24A. D – As Fig. 24A, for the oldest showers of 60–100,000 y age. The dashed line is that of Fig. 24A.

The evolution of other Taurid shower component streams was recently modeled by Tomko and Neslusan (2019). Different filaments were found to cross Earth's orbit that roughly correspond to the observed components. Table 4 gives the corresponding ages for each component.

In this case, the past orbit of the parent body is critical. Recently, an alternative explanation was found for why the broad Northern and Southern Taurids as a whole do not have matching distributions in node. Egal et al. (2021, 2022a, 2022b) found that the nodal distribution could be reproduced if comet 2P/Encke itself spent some time in the 7:2 mean-motion resonance with Jupiter in the recent past. This model suggested that some of the observed Taurid stream components are due to planetary perturbations on ejecta by 2P/Encke itself. From this model, the nominal ejection age of the dust contributing to the meteor shower seen today was given (Table 4).

Taken together, the Taurid Complex shows an increase of magnitude distribution index with age as shown in Fig. 22. Again, the data suggest a relationship proportional to the log of age, in this case best fit by a relation:

$$\text{Age (y)} = 450\, exp(1.14\, \chi) \quad (15)$$

This relation is much less steep than found for the Perseids (dashed

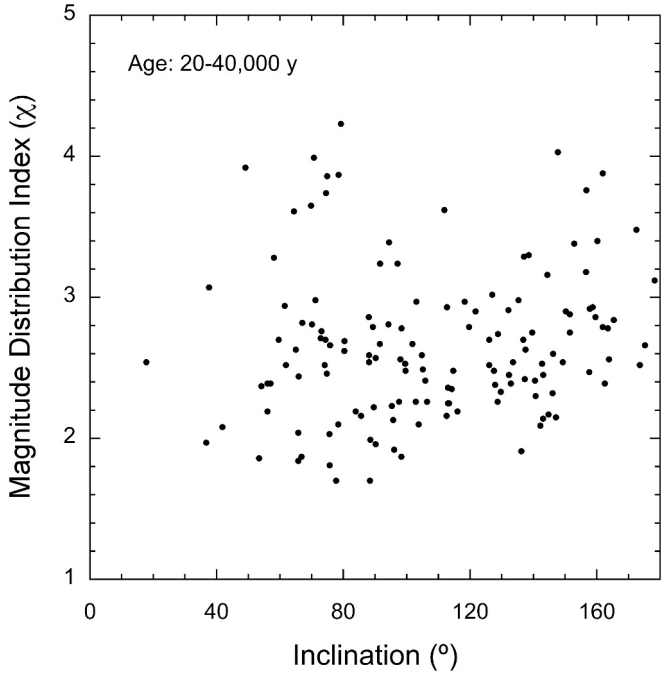

Fig. 25. Measured magnitude size distribution as a function of inclination, for all showers with calculated ages from dispersions in the range 20,000 to 40,000 years.

line). However, a similarly good relation linear fit would be the dashed line in Fig. 22, which is only a factor of two different than found for the Perseids (Eq. 14):

$$\text{Age (y)} = 20,000\sqrt{\text{q}}\,(\chi - 1.85) \tag{16}$$

4.3. Long-period comet showers

The dispersion of the 247 long-period comet meteoroid streams in our sample is expected to gradually increase over time. We fitted the observed dispersion of inclination, argument of perihelion and node to the calculated ages of the long-period dynamical models (Table 5), taking into account the apparent increase of dispersion with 1/q shown in Fig. 12, and found a relationship:

$$\text{Age (y)} \sim 12,000\ \text{q}\ \sigma_{\text{tot}} \tag{17}$$

Fig. 23 plots the age estimates based on the observed dispersion as a function of the measured magnitude distribution index. All long-period comet showers (•) and Mellish-type comets (+) with age estimates according to Eq. 17 are shown, those that were modeled and of which the dispersion was matched to the observed dispersions are shown as open circles.

Again, we identified an empirical age based on the magnitude distribution index χ. The Perseid-derived relationship (dashed line) is not a good fit to the distribution. We assume a common starting point, which may or may not be true for all streams, and set it at the lowest measured values of $\chi = 1.85$, the value where there is an equal combined cross sectional area per magnitude bin:

$$\text{Age (y)} = 40,000\ (\pm 8000)\sqrt{\text{q}}\,(\chi - 1.85) \tag{18}$$

This is the same relationship as Eq. 14 for the Perseids. We then noticed that a similar Age-σ relationship holds true for Mellish-type showers ($0.65 < T_J < 2$, $< 90°$). These relations differ in having a sqrt(q) dependence (see below), rather than q dependence as in Jenniskens (2023), and there being no longer a significant difference between Mellish type showers and long-period comet showers.

After using Eq. 17 with dispersion to define narrow ranges of age, the magnitude distribution index of those showers is plotted as a function of perihelion distance (Fig. 24) and inclination (Fig. 25) for all long-period comet and Mellish type showers. With each bin of age, the magnitude distribution index increases (Fig. 24).

In each age bin, the measured magnitude distribution index depends on perihelion distance, according to $1/\sqrt{q}$ (Fig. 24), but only if we ignore a number of high-χ showers near q ~ 1 AU that appear to have dispersions that do not represent the full dispersion of the shower. Taken together, the power-law fit implies a lower exponent of ~0.16–0.22.

There is no clear dependence on inclination (e.g., Fig. 25). A group of toroidal streams in prograde orbits appear not to belong in the 20–40,000 y age bracket, given that they have a high magnitude size distribution index. Perhaps the dispersion in Earth's path here underestimates the full dispersion of the stream due to the encounter geometry when ω ~ 0° or 180°.

5. Discussion

5.1. Physical mechanisms of long-period comet stream dispersions

Numerical integrations of long period comet meteoroid streams that remain in Earth's path indicate that the dispersions of orbital elements ι, ω and Ω of particles ejected from a single perihelion increase linearly in time, over a time interval between 10,000 and 120,000 years after ejection, following an initial brief exponential or power law inflation until the along-orbit spreading is complete.

The linear increase is due to random changes of the orbital elements in combination with the change in orbital periods of the particles over time starting from the initial comet orbital periods between 250 and 4000 years. Particles in short orbits are perturbed more than those in longer orbits. The particles that evolve to short ~120–250 y orbits are the most frequent to return to Earth.

Numerical simulations indicate that the dispersions of superpositions of ejecta from multiple perihelia also increase linearly with time, at similar rates. We surmise that there is a balance between loss and injection, with particles that are pumped to large periods being effectively lost to observation, and particles that drop to periods of under about 120 years being lost from the stream due to interaction with the inner solar system.

The orbital element dispersion growth of all elements increases fairly linearly with the orbital frequency (inverse of the period). The growth rate of the dispersion is generally larger for comets with lower perihelion, q. There is an additional change to the orbital elements due to precession/regression of the node that is also dependent on the orbital frequency. This contribution is less for higher inclined ($20° < \iota < 160°$) orbits.

The physical effects associated with this are discussed in Pilorz et al. (2023). First, the non-radial radiation forces are small for cm-sized ejecta over short time periods, so the dispersion growth is entirely due to gravitational effects for all practical purposes. There is a randomization due to perturbations as the various particles encounter the inner solar system at different epochs from each other, resulting in a rate of spread that is simply proportional to the number of orbits the particles have undergone.

Low inclined orbits have an increase in dispersion over time due to rotation of the nodal line, causing an azimuthal motion of the node, with particles in short orbits receiving many kicks and those in longer orbits being perturbed less. The rate of precession is effected by gravity acting over an orbit, hence also is inversely proportional to period.

The orbits with low q pass close to the Sun and experience perturbations due to the Sun's motion relative to the barycenter. These are in the form of a non-radial force with respect to the solar system barycenter, in which the torque should be expected to go generally as 1/q.

Altogether, we then expect the stream to reach a steady state in which particles are lost from the stream (either in reality, for the short period particles, or effectively, for the long period ones) at the rate they

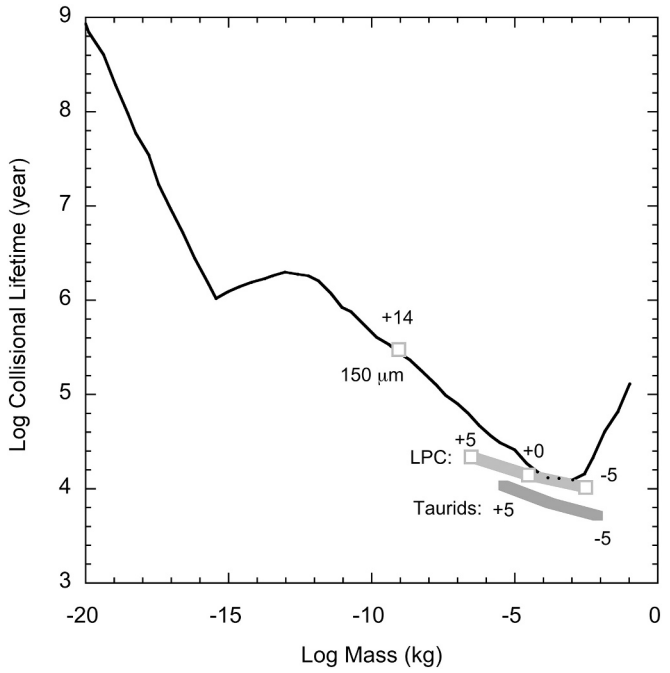

Fig. 26. Measured e-folding lifetime of meteoroids in long-period comet (LPC) and Taurid meteoroid streams (on a ^{10}log scale) compared to the MEMS2 collisional model for meteoroids in the orbit of comet 55P/Tempel-Tuttle (Soja, 2016). The MEMS2 lifetimes for Taurids are a factor of 3 lower. Also shown is the lifetime of 150 μm meteoroids at the peak of the mass influx curve according to Nesvorny et al. (2010).

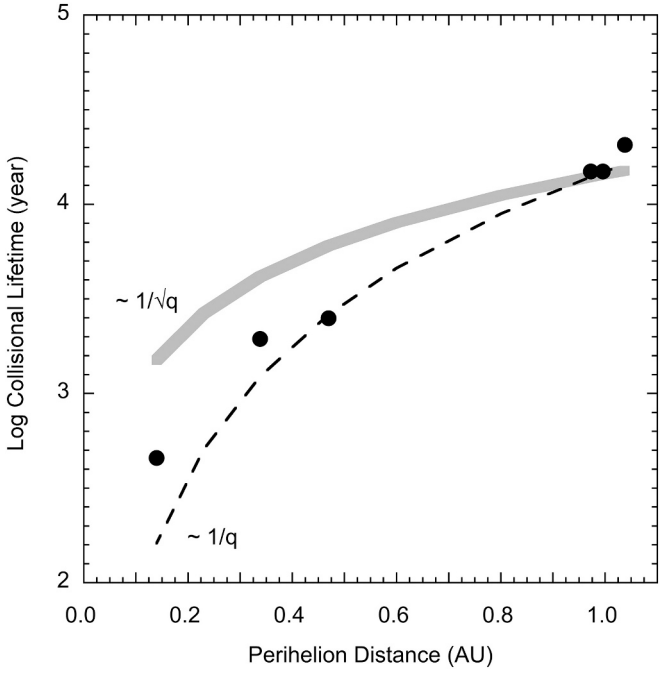

Fig. 27. Measured e-folding lifetime (on a ^{10}log scale) as a function of perihelion distance. The gray line is the $1/\sqrt{q}$ dependency observed, while solid points are the collisional lifetime from the IMEM2 model of 0-magnitude meteors that move in the orbits calculated by Soja et al. (2016). The dashed line shows a 1/q dependence for reference.

are injected or larger. As long as this is true, the rate of dispersion growth of particles ejected together at a single perihelion governs the rate of dispersion growth of the stream as a whole. These effects accumulate over time in inverse proportion to the orbital period, and in strength as the inverse of the distance of perihelion.

5.2. Lifetime at different masses: How meteoroid streams evolve in magnitude distribution index

What is the mm- and cm-sized meteoroid lifetime under different orbital conditions? The relationship of magnitude versus age of Eq. 18 implies a difference in meteoroid lifetime for meteoroids of different mass and size in a given stream. Meteoroids of a given size can break by erosive effects, increasing bins of smaller size at the expense of the larger sizes, or by catastrophic disruptions where the meteoroids of given size are disrupted into small fragments with sizes outside of the observed range. In either mechanism, Eq. 18 translates to lifetimes of about 10,300 years for magnitude −5 meteors (mass ~ 3 g), 14,000 years for +0 magnitude meteors (~0.03 g), and 21,700 years for magnitude +5 meteors (mass ~ 0.0003 g). This is shown in Fig. 26.

5.3. Implications for the mechanisms that limit the lifetime of cm-sized meteoroids

The lifetimes for long-period comet streams for q = 1 AU (Fig. 26) match well to the lifetime of cm-sized dust particles in a 55P/Tempel-Tuttle orbit as calculated from the IMEM2 meteoroid environment models (Soja et al., 2016, 2019). Any discrepancy between observation and model is well within the factor of two or so uncertainty in our age scale for long-period comets, suggesting that these ages are at most ~40% too low. Within this uncertainty, the results offer independent confirmation that the assumed meteoroid lifetimes for cm-sized particles in models like IMEM2 are correct, but it does not give insight into what is the main contributor to limiting the lifetime.

Orbital period does not seem to influence the meteoroid lifetime significantly. The lifetime of short-period Taurid shower meteoroids are only a factor of two lower than those of long-period comet showers based on Eq. 17. The orbital period of observed long-period comet meteoroids are mostly in the range 20–200 years (Fig. 8A), while Taurids have an about 3.3-y period. This too is consistent with the lifetimes calculated by Soja et al. (2016, 2019), who found very similar lifetimes for Leonids from comet 55P/Tempel-Tuttle with a 33.2-y orbit, Quadrantids from 2003 EH_1 with a 5.5-y orbit, and Draconids from comet 21P/Giacobini-Zinner with a 6.5-y orbit, all having orbits with a range of inclinations but similar mean q ~ 1 AU perihelion distance over the lifetime considered (Fig. 26).

The IMEM2 model results presented in Soja et al. predict a lifetime decrease for orbits with lower perihelion distances as shown in Fig. 27. The Grün et al. (1985) model predicts a q^{-1} dependence for the minimum mass that collisionally destroys a target mass due to increase of impact speeds closer to the Sun. The q-dependency in results from the model appears to be less steep than the 1/q (adopted in Jenniskens (2023), shown as a dashed line), but not quite as shallow as the $1/\sqrt{q}$ found here in Fig. 24. The about $q^{-0.77}$ dependency that results from the IMEM2 model may reflect the heliocentric dependence on dust density used in the model, which is consistent with results from radar-based orbital element surveys (e.g., Galligan and Baggaley, 2002).

If that heliocentric distribution of dust density in the IMEM2 model is correct, an $1/\sqrt{q}$ dependence would imply that the lifetime of cm-sized grains in the q < 1.02 AU range is not limited by collisions, but rather by properties proportional to temperature. The peak temperature (T) of meteoroids along their orbit is proportional to $T \sim 1/\sqrt{q}$, based on the Stefan-Boltzmann equation flux ~ T^4 and the fact that distance loss implies heat flux being proportional to $1/q^2$ (Poynting, 1904).

A dependence on temperature could mean that the meteoroid lifetime is limited by thermal stresses in the range 0.3 < q < 1.02 AU, given that it is generally assumed that the temperature gradient in a meteoroid $\Delta T \sim T$ (Delbo et al., 2014). The effect of these processes appears to be removing both the fluffy and dense particles from the population over

time, but results in a faster removal of the fluffy material. The preferential loss of fluffy particles over dense particles of the same mass in Fig. 20 implies a different lifetime. Fluffy particles have lower thermal conductivity and can more easily set up thermal stresses. Moreover, they have higher grain cross-sections due to a lower density. Densities of long-period comet and Mellish-type showers have a median value of $\rho \sim 0.69$ g/cm^3 for fluffy particles and $\rho \sim 2.06$ g/cm^3 for dense particles (Jenniskens, 2023). This corresponds to fluffy particles having a diameter 44% larger and a surface area difference of a factor of 2.

Near the Sun ($q < 0.3$ AU), the observed streams tend to be dominated by dense grains, poor or free in sodium (Borovicka et al., 2005; Jenniskens, 2023). Given that half of a cometary meteoroid is thought to consist of organic matter, it is likely that temperature plays a more direct role here. Around 0.3 AU, the grain temperature reaches 500 K, high enough to start sublimating some of the organic components that hold the mineral grains together. At $q = 0.2$ AU, that temperature has risen to about 610 K, at which much of organic matter is lost. The 50% condensation temperature for Na is about 960 K (Li et al., 2020), suggesting that if grain orbits evolve q to below 0.08 AU, all sodium will soon be lost.

No showers are observed for streams with $q < 0.03$–0.04 AU. At those distances, silicate materials sublimate by the heat of the Sun. At 0.04 AU, the grain temperature reached is ~1400 K, at which time mineral components will start to sublimate and the grains are lost. The 50% condensation temperature for the core elements Mg and Fe is about 1336 and 1335 K, respectively (Li et al., 2020).

5.4. Implications for understanding other parts of the mass influx curve

If the lifetime of cm-sized meteoroids with $q < 1.02$ AU is dominated by processes other than collisions, how can we understand the shape of the mass influx curve at Earth (Fig. 1)? Dynamical models of the zodiacal cloud need a lifetime of about 300,000 years for 100 μm meteoroids at the peak of the mass influx curve to explain the zodiacal infrared emission distribution (Nesvorny et al., 2010). That value compares well to the lifetime adopted in the MEMS2 model (Fig. 26). In the Grün et al. collision model, the longer lifetimes for smaller sizes reflect a relative lower abundance of small impactor particles. On the other hand, smaller grains are less susceptible to thermal stresses because it is harder to set up a temperature gradient across the grain.

Temperature will affect the lifetime of small grains on orbits with $q < 0.3$ AU in a different way than for large cm-sized grains. Their lifetime is relatively longer because small grains are more efficient in radiating heat and more efficient at scattering light. Moreover, as they warm, their structure and chemical composition will change, which will also change their optical properties, increasing albedo with the loss of organics, resulting in less absorption of sunlight.

The longer lifetimes for particles larger than 1-cm may have a non-collision rate related reason also. The upward curvature in the collisional lifetime model for meteors brighter than −5 magnitude may not be due to fewer suitably-sized impactors at larger sizes, but rather the changing composition of the meteoroids, from being dominated by cometary matter for meteors fainter than −5 magnitude to being dominated by asteroidal matter for meteors brighter than −15 magnitude. While asteroidal objects of 0.1 to 1-m in size are known to exist and survive for up to 100 million years, based on meteorites that fall on the ground, there are few large cometary boulders in the sporadic population and most are associated with the Leonid shower (Ozerov et al., 2014). Larger objects in the Taurid complex often belong to the s-Taurids, a relatively young shower component (Devillepoix et al., 2019). The bright Leonid fireballs, too, may be part of such a “Filament” component, a young stream.

6. Conclusions

The dispersion of meteoroid streams from long-period comets with perihelion distances $0.3 < q < 1.02$ AU increases in time and at a faster rate for streams with shorter perihelion distances, proportional to 1/q. When long period comet showers age, their magnitude size distribution increases, the fraction of dense materials increases, and their mean densities increase. Low-density materials are lost before high density materials.

Showers with shorter perihelion distances $q < 0.2$ AU, and a fraction of $q < 0.3$ AU, appear to be mostly young. The meteoroids in these young streams are already highly modified, with a high fraction of dense materials, poor or free in sodium, and predominantly high lightcurve shape parameter F-values. This includes meteoroid streams on both short period and long period orbits.

Based on literature data on the age of stream components, the Taurids of comet 2P/Encke (3.3-y orbit, approaching the Sun to ~0.34 AU) show a linear increase of χ with age, while the Perseids of comet 109P/Swift-Tuttle (133-y orbit, approaching the Sun to ~0.96 AU) hint at the same, depending on the correctness of the various proposed age estimates.

Based on new dynamical modeling, we derived age estimates for long-period comet showers based on their observed dispersions. Modeled dispersions increase more or less linearly with age for ages of about 10,000 to 120,000 years, after an initial rapid increase when grains first spread along the orbit. Perihelion distance does not change much over time, but low-inclination showers show strong precession in the form of a rotation of the nodal line, so they remain in Earth’s path only for a short period of time. We confirm that low perihelion distance streams spread faster, proportional to 1/q. Taking this into account, we again find a linear increase of χ with age, at a rate similar to that found for the Perseids, and only a factor of two slower than that found for the Taurids.

While the lifetime of grains is calculated correctly in current zodiacal cloud models, to within a factor of two, the reason for those lifetimes is not due to grain-grain collisions. When restricting the sample of observed showers in narrow groups of age (based on dispersion), we find that in each age group the value of χ increases towards smaller values of q. The magnitude distribution index is proportional to $1/\sqrt{q}$. This shallow dependence on perihelion distance is less steep than in current meteoroid environment models that assume that the meteoroid lifetime is limited by collisions.

Instead, our $1/\sqrt{q}$ dependence on perihelion distance suggests that the meteoroid lifetime of grains that move in orbits with $0.3 < q < 1.02$ AU is limited by the peak grain temperature along the orbit. This is possible if that lifetime is limited by thermal stresses. For perihelion distances $q < 0.3$ AU, temperature may be a more direct factor in that sublimation of organic compounds can limit the lifetime of the grains. For $q < 0.08$ AU, minerals containing sodium are lost from the grains and for $q < 0.04$ AU the core minerals sublimate. No meteoroid streams are observed with $q < 0.03$ AU.

We conclude that processes other than grain-grain collisions are responsible for the loss of cm-sized grains from meteoroid streams and the zodiacal cloud for particles on orbits with $q < 1.02$ AU.

Funding

This research was performed as part of NASA’s Solar System Workings grant 80NSSC19K0563 and Emerging Worlds grant NNH18ZDA001N. Support for the development and operation of CAMS over the years was provided by earlier NASA grants and individual networks are supported by local grants, notably CAMS Turkey by TUBITAK (Project code MFAG/113F035). This work is supported by NASA under Contract NNM10AA11C issued through the New Frontiers Program.

CRediT authorship contribution statement

Peter Jenniskens: Writing – original draft, Visualization,

Supervision, Resources, Project administration, Methodology, Investigation, Funding acquisition, Formal analysis, Data curation, Conceptualization. **Stuart Pilorz:** Writing – original draft, Software, Methodology, Investigation. **Peter S. Gural:** Writing – review & editing, Software, Methodology, Data curation. **Dave Samuels:** Writing – review & editing, Software, Methodology, Data curation. **Steve Rau:** Writing – review & editing, Software, Methodology, Data curation. **Timothy M.C. Abbott:** Writing – review & editing, Data curation. **Jim Albers:** Writing – review & editing, Data curation. **Scott Austin:** Writing – review & editing, Data curation. **Dan Avner:** Writing – review & editing, Data curation. **Jack W. Baggaley:** Writing – review & editing, Data curation. **Tim Beck:** Writing – review & editing, Data curation. **Solvay Blomquist:** Writing – review & editing, Data curation. **Mustafa Boyukata:** Writing – review & editing, Data curation. **Martin Breukers:** Writing – review & editing, Data curation. **Walt Cooney:** Writing – review & editing, Data curation. **Tim Cooper:** Writing – review & editing, Data curation. **Marcelo De Cicco:** Writing – review & editing, Data curation. **Hadrien Devillepoix:** Writing – review & editing, Data curation. **Eric Egland:** Writing – review & editing, Data curation. **Elize Fahl:** Writing – review & editing, Data curation. **Megan Gialluca:** Writing – review & editing, Data curation. **Bryant Grigsby:** Writing – review & editing, Data curation. **Toni Hanke:** Writing – review & editing, Data curation. **Barbara Harris:** Writing – review & editing, Data curation. **Steve Heathcote:** Writing – review & editing, Data curation. **Samantha Hemmelgarn:** Writing – review & editing, Data curation. **Andy Howell:** Writing – review & editing, Data curation. **Emmanuel Jehin:** Writing – review & editing, Data curation. **Carl Johannink:** Writing – review & editing, Data curation. **Luke Juneau:** Writing – review & editing, Data curation. **Erika Kisvarsanyi:** Writing – review & editing, Data curation. **Philip Mey:** Writing – review & editing, Data curation. **Nick Moskovitz:** Writing – review & editing, Data curation. **Mohammad Odeh:** Writing – review & editing, Data curation. **Brian Rachford:** Writing – review & editing, Data curation. **David Rollinson:** Writing – review & editing, Data curation. **James M. Scott:** Writing – review & editing, Data curation. **Martin C. Towner:** Writing – review & editing, Data curation. **Ozan Unsalan:** Writing – review & editing, Data curation. **Rynault van Wyk:** Writing – review & editing, Data curation. **Jeff Wood:** Writing – review & editing, Data curation. **James D. Wray:** Writing – review & editing, Data curation. **Jérémie Vaubaillon:** Writing – review & editing, Software. **Dante S. Lauretta:** Writing – review & editing, Funding acquisition.

Declaration of competing interest

The authors declare that they have no known competing financial interests or personal relationships that could have appeared to influence the work reported in this paper.

Data availability

The meteoroid stream orbital elements and dispersions, their size distribution index, lightcurve shape parameters, densities and fraction of dense materials were published in Jenniskens (2023) and will be made available in digital form through the NASA/PDS node for Small Solar System Bodies. That node will also contain data on a number of long-period comet meteoroid stream models generated as part of this study.

Acknowledgements

We thank Matt Tiscareno of the SETI Institute for the initial setup of the PINTEM software and Sean Hsu of LASP/University of Colorado for helpful discussions. We thank the CAMS station operators for building and maintaining the global CAMS camera networks and the SETI Institute for program management and maintaining the IT environment for data processing and reporting.

References

Abedin, A., Spurny, P., Wiegert, P., Pokorny, P., Borovicka, J., Brown, P., 2015. On the age and formation mechanism of the core of the Quadrantid meteoroid stream. Icarus 261, 100–117.
Acton, C., Bachman, N., Semenov, B., Wright, E., 2017. A look toward the future in the handling of space science mission geometry. Planet. Space Sci. 150, 9–12.
Adreic, Z., Segon, D., 2010. The first year of Croatian meteor network. In: Kaniansky, S., Zimnikoval, P. (Eds.), Proceedings of the International Meteor Conference, Sachticka, Slovakia, 18-21 Sep. 2008. International Meteor Organization, Mechelen, pp. 16–23.
Asher, D.J., Izumi, K., 1998. Meteor observations in Japan: new implications for a Taurid meteoroid swarm. Monthly Notices of the Royal Astronomical Society 297, 23–27.
Bardyn, A., Baklouti, D., Cottin, H., Fray, N., Briois, C., Paquette, J., Stenzel, O., Engrand, C., Fischer, H., Hornung, K., Isnard, R., Langevin, Y., Lehto, H., Le Roy, L., Ligier, N., Merouane, S., Modica, P., Orthous-Daunay, F.R., Rynö, J., Schulz, R., Silén, J., Thirkell, L., Varmuza, K., Zaprudin, B., Kissel, J., Hilchenbach, M., 2017. Carbon-rich dust in comet 67P/Churyumov-Gerasimenko measured by COSIMA/Rosetta. MNRAS 469, S712–S722.
Beech, M., Murray, I.S., 2003. Leonid meteor light-curve synthesis. Monthly Notices of the Royal Astronomical Society 345, 696–704.
Bentley, M.S., Schmied, R., Mannel, T., Torkar, K., Jeszensky, H., Romstedt, J., Levasseur-Regourd, A.C., Weber, I., Jessberger, E.K., Ehrenfreund, P., Koeberl, C., Havens, O., 2016. Aggregate dust particles at comet 67P/Churyumov-Gerasimenko. Nature 537, 73–75.
Borovicka, J., Koten, P., Spurny, P., Bocek, J., Stork, R., 2005. A survey of meteor spectra and orbits: evidence for three populations of Na-free meteoroids. Icarus 174, 15–30.
Borovicka, J., Spurny, P., Koten, P., 2008. Atmospheric deceleration and light curves of Draconid meteors and implications for the structure of cometary dust. Astron. Astrophys. 473, 661–672.
Brown, P., Jones, J., 1998. Simulation of the formation and evolution of the Perseid meteoroid stream. Icarus 133, 36–68.
Brown, P., Wong, D.K., Weryk, R.J., Wiegert, P., 2010. A meteoroid stream survey using the Canadian Meteor Orbit Radar. II: identification of minor showers using a 3D wavelet transform. Icarus 207, 66–81.
Brownlee, D.E., Tsou, P., Aléon, J., et al., 2006. Comet 82P/Wild 2 under a microscope. Science 314, 1711–1716.
Buccongello, N., Brown, P.G., Vida, D., 2023. A physical survey of meteoroid streams: Comparing cometary reservoirs. In: ACM 2023, LPI Contrib. No. 2851, Abstract 2464.
Buccongello, N., Brown, P.G., Vida, D., Pinhas, A., 2024. A physical survey of meteoroid streams: comparing cometary reservoirs. Icarus 410 article id.115907.
Ceplecha, Z., McCrosky, R.E., 1976. Fireball end heights: a diagnostic for the structure of meteoric material. J. Geophys. Res. 81, 6257–6275.
Ceplecha, Z., Borovicka, J., Graham, E.W., Revelle, D.O., Hawkes, R.L., Porubcan, V., Simek, M., 1998. Meteor phenomena and bodies. Space Sci. Rev. 84, 327–471.
Chesley, S.R., French, A.S., Davis, A.B., Jacobson, R.A., Brozovic, M., Farnocchia, D., et al., 2020. Trajectory and estimation for particles observed in the vicinity of (101955) Bennu. JGR Planets 125 article id. e2019JE006363.
Crovisier, J., 1997. Infrared observations of volatile molecules in comet Hale-Bopp. Earth Moon Planets 79, 125–143.
Curdt, W., Keller, H.U., 1990. Large dust particles along the Giotto trajectory. Icarus 86, 305–313.
Delbo, M., Libourel, G., Wilkerson, J., Murdoch, N., Michel, P., Ramesh, K.T., Ganino, C., Verati, C., Marchi, S., 2014. Nature 508, 233–237.
Devillepoix, H.A.R., Bland, P.A., Jenniskens, P., Samsom, E.K., Towner, M.C., Cupak, M., Howie, R.M., Hartig, B.A.D., Jansen-Sturgeon, T., Paxman, J., 2019. Taurid stream #628: a reservoir of large cometary impactors. Planetary Science Journal 2, 223–236.
Divine, N., 1993. Five populations of interplanetary meteoroids. J. Geophys. Res. Planets 98, 17029–17048.
Egal, A., Wiegert, P., Brown, P.G., Spurny, P., Borovicka, J., Valsecchi, G.B., 2021. A dynamical analysis of the Taurid complex: evidence for past orbital convergences. Montly Notices of the Royal Astronomical Society 507, 2568–2591.
Egal, A., Wiegert, P., Brown, P.G., 2022a. A proposed alternative dynamical history for 2P/Encke that explains the Taurid meteoroid complex. Monthly Notices of the Royal Astronomical Society 515, 2800–2821.
Egal, A., Brown, P.G., Wiegert, P., Kipreos, Y., 2022b. An observational synthesis of the Taurid meteor complex. Monthly Notices of the Royal Astronomical Society 512, 2318–2336.
Everhart, E., 2014. An efficient integrator that uses gauss-Radau spacings. In: Carusi, A., Valsecchi, G.B. (Eds.), Dynamics of comets: Their origin and evolution. Proceedings of IAU Colloq. 83, held in Rome, Italy, June 11–15, 1984, 115. Reidel, Astrophysics and Space Scienc Library, Dordrecht, pp. 185–202.
Fienga, A., Manche, H., Laskar, J., Castineau, M., 2008. INPOP06: a new numerical planetary ephemeris. Astronomy & Astrophysics 477, 315–327.
Flynn, G.J., 2001. Atmospheric entry heating of interplanetary dust. In: Peucker-Ehrenbrink, B., Schmitz, B. (Eds.), Accretion of Extraterrestrial Matter throughout Earth's History. Kluwer Academic/Plenum Publishers, New York, pp. 107–127.
Fulle, M., Levasseur-Regourd, A.C., McBride, N., Hadamcik, E., 2000. In situ dust measurements from within the coma of 1P/Halley: first-order approximation with a dust dynamical model. Astron. J. 119, 1968–1977.
Fulle, M., Della, Corte V., Rotundi, A., Green, S.F., Accolla, M., Colangeli, L., Ferrari, M., Ivanovski, S., Sordini, R., Zakharov, V., 2017. The dust-to-ices ratio in comets and Kuiper belt objects. Monthly Notices of the Royal Astronomical Society 469, S45–S49.

Fulle, M., Bertini, I., Della, Corte V., Güttler, C., Ivanovski, S., La Forgnia, F., Lasue, J., Levasseur-Regourd, A.C., Marzari, F., Moreno, F., Mottola, S., Naletto, G., Palumbo, P., Rinaldi, G., Rotundi, A., Sierks, H., Barbieri, C., Lamy, P.L., Rodrigo, R., Koschny, D., Rickman, H., Barucci, M.A., Bertaux, J.-L., Bodewits, D., Cremonese, G., Da Deppo, V., Davidsson, B., Debei, S., De Cecco, M., Deller, J., Fornasier, S., Groussin, O., Gutiérrez, P.J., Hviid, H.S., Ip, W.H., Jorda, L., Keller, H.U., KNollenberg, J., Kramm, J.R., Kührt, E., Küppers, M., Lara, M.L., Lazzarin, M., López-Moreno, J.J., Shi, X., Thomas, N., Tubiana, C., 2018. The phase function and density of the dust observed at comet 67P/Churyumov-Gerasimenko. Monthly Notices of the Royal Astronomical Society 476, 2835–2839.

Galligan, D.P., Baggaley, W.J., 2002. Determination of the spatial distribution of the solar system meteoroid population using AMOR. ESA SP 500 (279–212).

Gastineau, M., Laskar, J., Manche, H., Fienga, A., 2015. CALCEPH: planetary ephemeris files access code. Astrophysics Source Code Library (record asci:1505.001).

Grün, E., Zook, H.A., Fechtig, H., Giese, R.H., 1985. Collisional balance of the meteoric complex. Icarus 62, 244–272.

Hajduková, M., Neslusan, L., 2017. Regular and transitory showers of comet C/1979 Y1 (Bradfield). Astronomy & Astrophyisics 605 id. A36, 13pp.

Hajduková, M., Neslusan, L., 2019. Modeling of the meteoroid streams of comet C/1975 T2 and λ-Ursae Majorids. Astronomy & Astrophysics 627, A73–A80.

Hajduková, M., Neslusan, L., 2021. Modeling the meteoroid streams of comet C/1861 G1 (Thatcher). Planet. Space Sci. 203 id. 105246.

Hajduková, M., Rudawska, R., Kornos, L., Toth, J., 2015. April ρ Cygnids and comet C/1917 F1 Mellish. Planetary & Space Science 118, 28–34.

Hamid, S.E., 1954. In: A. C. B. Lovell, Meteor astronomy. Clarendon Press, Oxford, p. 429.

Haranas, I., Ragos, O., Gkigkitzis, I., Kotsireas, I., Martz, C., Van Middekoop, S., 2018. The Poynting-Robertson effect in the Newtonian potential with a Yukawa correction. Astrophys. Space Sci. 36 article id. 3, 11 pp.

Harris, N.W., Yau, K.K.C., Hughes, D.W., 1995. The true extent of the nodal distribution of the Perseid meteoroid stream. MNRAS 273, 999–1015.

Hawkins, G.S., 1963. The Harvard radio meteor project. Smithsonian Contributions to Astrophysics 7, 53–62.

Jacchia, L.G., Verniani, F., Briggs, R.E., 1967. Analytics of the atmospheric trajectories of 413 preciese photographic meteors. Smiths. Contrib. Astrophys. 10, 1–139.

Jenniskens, P., 2006. Meteor showers and their parent comets. Cambridge University Press, Cambridge, p. 790.

Jenniskens, P., 2023. Atlas of Earth's meteor showers. Elsevier, Amsterdam, p. 838.

Jenniskens, P., Nénon, Q., 2016. CAMS verification of single-linked high-threshold D-criterion detected meteor showers. Icarus 266, 371–383.

Jenniskens, P., Vaubaillon, J., 2010. Minor planet 2002 EX_{12} (=169 P/NEAT) and the alpha Capricornid shower. Astronomical Journal 139, 1822–1830.

Jenniskens, P., Betlem, H., de Lignie, M., ter Kuile, C., van Vliet, M.C.A., Van't Leven, J., Koop, M., Morales, E., Rice, T., 1998. On the unusual activity of the Perseid meteor shower (1989-96) and the dust trail of comet 109P/Swift-Tuttle. Montly Notices of the Royal Astronomical Society (or do it systematically MNRAS in all of references) 301, 941–954.

Jenniskens, P., de Kleer, K., Vaubaillon, J., Trigo-Rodriguez, J.M., Madiedo, J.M., Haas, R., ter Kuile, C.R., Miskotte, K., Vandeputte, M., Johannink, C., Bus, P., Van't Leven, J., Jobse, K., Koop, M., 2008. Leonids 2006 observations of the tail of trails: where is the comet fluff? Icarus 196, 171–183.

Jenniskens, P., Vaubaillon, J., Atreya, P., Vachier, F., Barentsen, G., 2009. Leonid meteors 2009. In: Green, D.W.E. (Ed.), Central Bureau Electronic Telegrams 2064. IAU Central Bureau for Electronic Telegrams, Boston, 1 pp.

Jenniskens, P., Gural, P.S., Dynneson, L., Grigsby, B.J., Newman, K.E., Borden, M., Koop, M., Holman, D., 2011. CAMS: cameras for Allsky meteor surveillance to establish minor meteor showers. Icarus 216, 40–61.

Jenniskens, P., Nénon, Q., Gural, P.S., Albers, J., Haberman, B., Johnson, B., Morales, R., Grigsby, B.J., Samuels, D., Johannink, C., 2016a. CAMS newly detected meteor showers and the sporadic background. Icarus 266, 384–409.

Jenniskens, P., Nénon, Q., Gural, P.S., Albers, J., Haberman, B., Johnson, B., Holman, D., Morales, R., Grigsby, B.J., Samuels, D., Johannink, C., 2016b. CAMS confirmation of previously reported meteor showers. Icarus 266, 355–370.

Jenniskens, P., Nénon, Q., Albers, J., Gural, P.S., Haberman, B., Holman, D., Grigsby, B. J., Samuels, D., Johannink, C., 2016c. The established meteor showers as observed by CAMS. Icarus 266, 331–354.

Jenniskens, P., Baggaley, J., Crumpton, I., Aldous, P., Pokorny, P., Janches, D., Gural, P. S., Samuels, D., Albers, J., Howell, A., Johannink, C., Breukers, M., Odeh, M., Moskovitz, N., Collison, J., Ganju, S., 2018. A survey of southern hemisphere meteor showers. Planetary & Space Science 154, 21–29.

Jenniskens, P., Lauretta, D.S., Towner, M.C., Heathcote, S., Jehin, J., Hanke, T., Cooper, T., Baggaley, J.W., Howell, J.A., Johannink, C., Breukers, M., Odeh, M., Moskovitz, N., Juneau, L., Beck, T., De Cicco, M., Samuels, D., Rau, S., Albers, J., Gural, P.S., 2021. Meteor showers from known long period comets. Icarus 365 article id. 114469.

Kanamori, T., 2009. A meteor shower catalog based on video observations in 2007–2008. JIMO 37, 55–62.

Kondrat'eva, E.D., Reznikov, E.A., 1985. Comet Tempel-Tuttle and the Leonid meteor swarm. Solar Sysem Research 19, 96–101.

Kornos, L., Koukal, J., Piffl, R., Toth, J., 2013. Database of meteoroid orbits from several European video networks. In: Gijssens, M., Roggemans, P. (Eds.), Proceedings of the International Meteor Conference, La Palma, Canary Islands, Spain, 20-23 Sep. 2012. International Meteor Organization, Mechelen, pp. 21–25.

Koschny, D., Drolshagen, E., Drolshagen, S., Kretschmer, J., Ott, T., Drolshagen, G., Poppe, B., 2017. Flux densities of meteoroids derived from optical double-station observations. Planet. Space Sci. 143, 230–237.

Koten, P., Capek, D., Spurny, P., Vaubaillon, J., Popek, M., Shrbeny, L., 2017. September epsilon Perseid cluster as a result of orbital fragmentation. Astronomy & Astrophysics 600 id. A74, 5pp.

Koten, P., Capek, D., Midtskogen, S., Shrbeny, L., Spurny, P., Hankey, M., 2024. Properties, age, and origin of a huge meteor cluster observed over Scandinavia on 30 October 2022. Astronomy & Astrophysics 683 (A5), 10.

Langevin, Y., Hilchenbach, M., Ligier, N., Merouane, S., Hornung, K., Engrand, C., Schulz, R., Kissel, J., Rynö, J., Eng, P., 2016. Typology of dust particles collected by the COSIMA mass spectrometer in the inner coma of 67P/Churyumov Gerasimenko. Icarus 271, 76–97.

Lasue, J., Levasseur-Regourd, A.-C., Renard, J.-B., 2020. Zodiacal light observations and its link with cosmic dust: a review. Planetary Space Science 190, 104973.

Lauretta, D.S., Hergenrother, C.W., Chesley, S.R., Leonard, J.M., Pelgrift, J.Y., Adam, C. D., Al, Asad M., Antreasian, P.G., Ballouz, R.-L., Becker, K.J., Bennett, C.A., Bos, B.J., Bottke, W.F., Brozovic, M., Campins, H., Connolly Jr., H.C., Daly, M.G., Davis, A.B., de León, J., DellaGiustina, D.N., Drouet, d'Aubigny C., Dworkin, J.P., Emery, J.P., Farnoccia, D., Glavin, D.P., Golish, D.R., Hartzell, C.M., Jacobson, R.A., Jawin, E.R., Jenniskens, P., Kidd, J.N., Lessac-Chenen, E.J., Li, Y.-Y., Libourel, G., Licandro, J., Lionis, A.J., Maleszeweksi, C.K., Manzoni, C., May, B., McCarthy, L., McMahon, J.W., Michel, P., Molaro, J.L., Nelson, D.S., Owen, J.W.M., Rizk, B., Roper, H.L., Rozitis, B., Sah, E.M., Scheeres, D.J., Seabrook, J.A., Selznick, S.H., Takahashi, Y., Thuillet, F., Tricarico, P., Vokrouhlicky, D., Wolner, C.W.V., 2019. OSIRIS-REx discovery of particle ejection from asteroid (101955) Bennu. Science 366, 3544–3546.

Levasseur-Regourd, A.-C., Agarwal, J., Cottin, H., Engrand, C., Flynn, G., Fulle, M., Gombosi, T., Langevin, Y., Lasue, J., Mannel, T., Merouane, S., Poch, O., Thomas, N., Westphal, A., 2018. Cometary dust. Space Science Review 214 article id. 64, 56 pp.

Li, M., Huang, S., Petaev, M., Zhu, Z., Steffen, J., 2020. Dust condensation in evolving discs and the composition of meteorites, planetesimals, and planets. Monthly Notices of the Royal Astronomical Society 495, 2543–2553.

Love, S.G., Brownlee, D.E., 1993. A direct measurement of the terrestrial mass accretion rate of cosmic dust. Science 262, 550–553.

McNaught, R.H., Asher, D.J., 1998. Leonid dust trails and meteor storms. JIMO 27, 85–102.

Moorhead, A.V., Wiegert, P.A., Cooke, W.J., 2014. The meteoroid fluence at Mars due to comet C/2013 A1 (Siding Spring). Icarus 231, 13–21.

Moorhead, A.V., Milbrandt, K., Kingery, A., 2023. A library of meteoroid environments encountered by spacecraft in the inner solar system. Advances in Space Research 72, 4582–4595.

Neslusan, L., Hajduková, M., 2018. Meteor showers from comet C/1964 N1 (Ikeya). Astronomy & Astrophysics 616 id.A162, 8pp.

Neslusan, L., Hajduková, M., 2019. Long-period comet C/1961 A1 (Ikeya), the probable parent body of π-Hydrids, δ-corvids, November α-Sextantids, and θ-Leonids. Astronomy & Astrophyiscs 631 id.A112, 10pp.

Neslusan, L., Hajduková, M., 2020. The relationship between comet C/1853 G1 (Schweizer) and the γ-Aquilids and 52 Herculids meteor showers. Monthly Notices of the Royal Astronomical Society 498, 1013–1022.

Neslusan, L., Hajduková, M., 2021. Meteoroid stream of comet C/1961 T1 (Seki) and its relation to the December -Virginids and -Sagittariids. Astronomical Journal 162 id. 20, 9pp.

Nesvorny, D., Jenniskens, P., Levison, H.F., Bottke, W.F., Vokrouhlicky, D., Gounelle, M., 2010. Cometary origin of the zodiacal cloud and carbonaceous micrometeorites. Implications for hot debris disks. Astrophysical Journal 713, 816–836.

Nesvorny, D., Janches, D., Vokrouhlicky, D., Pokorny, P., Bottke, W.F., Jenniskens, P., 2011. Dynamical model for the zodiacal cloud and sporadic meteors. ApJ 743, 729–745.

Ozerov, A., Smith, J.C., Dotson, J.L., Longenbaugh, R.S., Morris, R.L., 2014. GOES GLM, biased bolides, and debiased distributions. Icarus 408 id. 115843.

Piers, P.A., Hawkes, R.L., 1993. An unusual meteor cluster observed by image-intensified video. JIMO 21, 168–174.

Pilorz, S., Jenniskens, P., Vaubaillon, J., 2023. Age-dependent orbital dispersion growth of long period comet meteor showers. In: Asteroids, Comets, Meteors 2023. Flagstaff, AZ, abstract id# 2484.

Pokorny, P., Vokrouhlicky, D., Nesvorny, D., Campbell-Brown, M., Brown, P., 2014. Dynamical model for the toroidal sporadic meteors. Astrophysical Journal 789 article id. 25, 20 pp.

Poynting, J.H., 1904. Radiation in the solar system: its effect on temperature and its pressure on small bodies. Proceedings of the Royal Society 72, 525–552.

Reynolds, R.J., Madsen, G.J., Moseley, S.H., 2004. New measurements of the motion of the zodiacal dust. The Astrophysical Journal 612, 1206–1213.

Rowan-Robbinson, M., May, B., 2013. An improved model for the infrared emission from the zodiacal dust cloud: cometary, asteroidal and interstellar dust. Monthly Notices of the Royal Astronomical Society 429, 2894–2902.

Rudawska, R., Jenniskens, P., 2014. New meteor showers identified in the CAMS and SonotaCo meteoroid orbit surveys. In: Jopek, T., Rietmeijer, F.J.M., Watanabe, J., Williams, I.P. (Eds.), Meteoroids 2013, Proceedings of the Astronomical Conference Held at A.M. University, Poznan, Poland, Aug 26–30, 2013. A. M. University Press, Poznan, pp. 217–224.

Soja, R.H., Schwarzkopf, G.J., Sommer, M., Vaubaillon, J., Albin, T., Rodmann, J., Grün, E., Srama, R., 2016. Collisional lifetimes of meteoroids. In: Roggemans, A., Roggemans, P. (Eds.), Proceedings of the International Meteor Conference, Egmond, the Netherlands, 2-5 June 2016, pp. 284–286.

Soja, R.H., Grün, E., Strub, P., Sommer, M., Millinger, M., Vaubaillon, J., Alius, W., Camodeca, G., Hein, F., Laskar, J., Gastineau, M., Fienga, A., Schwarzkopf, G.J., Herzog, J., Gutche, K., Skuppin, N., Srama, R., 2019. IMEM2: a meteoroid

environment model for the inner solar system. Astron. Astrophys. 628 id. A109, 13pp.
Spurny, P., Borovicka, J., Mucke, H., Svoren, J., 2017. Discovery of the new branch of the Taurid meteoroid stream as a real source of potentially hazardous bodies. Astronomy & Astrophysics 605 id.A68, 25pp.
Tomko, D., Neslusan, L., 2019. Meteoroid-stream complex originating from comet 2P/Encke. Astronomy & Astrophyics 623, A13–A37.
Tsuchiya, C., Sato, M., Watanabe, J.-I., Moorhead, A.V., Moser, D.E., Brown, P.G., Cooke, W.J., 2017. Correction effect to the dispersion of radiant point in case of low velocity meteor showers. Planetary Space Science 143, 142–146.
Vaubaillon, J., Colas, F., Jordan, L., 2005. A new method to predict meteor showers. I. Description of the model. Astronomy & Astrophysics 2005, 751–760.
Vaubaillon, J., Loir, C., Clocan, C., Kandeepan, M., Millet, M., Cassagne, A., Lacassagne, L., Da Fonseca, P., Zander, F., Buttsworth, D., Loehle, S., Toth, J., Gray, S., Moingeon, A., Rambaux, N., 2023. A 2022 τ-Herculid meteor cluster from an airborne experiment: automated detection, characterization, and consequences for meteoroids. Astronomy & Astrophysics 670 id.A86, 6 pp.
Vida, D., Gural, P.S., Brown, P.G., Campbell-Brown, M., Wiegert, P., 2020. Estimating trajectories of meteors: an observational Monte Carlo approach – I. Theory. Monthly Notices of the Royal Astronomical Society 491, 2688–2705.
Vida, D., Segon, D., Gural, P.S., Brown, P.G., McIntyre, M.J., Dijkema, P., 2021. The Global Meteor Network – methodology and first results. Monthly Notices of the Royal Astronomical Society 506, 5046–5074.
Westphal, A.J., Fakra, S.C., Gainsforth, Z., Marcus, M.A., Ogliore, R.C., Butterworth, A.L., 2009. Mixing fraction of inner solar system material in comet 81P/Wild 2. Astrophysical Journal 694, 18–28.
Wiegert, P., Vaubaillon, J., Campbell-Brown, M., 2009. A dynamical model of the sporadic meteoroid complex. Icarus 201, 295–310.
Wooden, D.H., Harker, D.E., Woodward, C.E., Butner, H.M., Koike, C., Witteborn, F.C., McMurtry, C.W., Craig, W., 1999. Silicate mineralogy of the dust in the inner coma of comet C/1995 O1 (Hale-Bopp) pre and postperihelion. Astrophysical Journal 517, 1034–1058.
Yau, K., Yeomans, D.K., Weissman, P., 1993. The past and future motion of comet P/Swift-Tuttle. Monthly Notices of the Royal Astronomical Society 266, 305–316.
Yeomans, D.K., Yau, K.K., Weissman, P.R., 1996. The impending appearance of comet Temple-Tuttle and the Leonid meteors. Icarus 124, 407–413.